

Supplementary material

Matteo Puglini^{1,2}, Victor Brovkin¹, Pierre Regnier², and Sandra Arndt²

¹Land in the Earth System, Max Planck Institute for Meteorology, Hamburg, Germany

²BGeosys, Department Geoscience, Environment & Society (DGES), Université Libre de Bruxelles, Brussels, Belgium

Correspondence: Matteo Puglini (matteo.puglini@mpimet.mpg.de)

S1 From continuity equation to advection-diffusion-reaction equation

Each equation (one per species i) is a specific generalization of a continuity equation with fluxes \mathcal{F}_i , related to the transport processes, and sources/sinks \mathcal{S}_i related to the biogeochemical reactions. It reads:

$$\frac{\partial \xi(z) C_i(z, t)}{\partial t} = -\frac{\partial \mathcal{F}_i(z, t)}{\partial z} + \mathcal{S}_i(z, t). \quad (\text{S1})$$

- 5 Where $C_i(z, t)$ is the concentration of the species i (referred to porewater volume if it is a dissolved species or solid matrix volume if it is a solid species) and $\xi(z)$ is the term accounting for this, *i.e.* the porosity $\xi = \varphi$ in case of a dissolved species or the solid fraction $\xi = \varphi_s = 1 - \varphi$ in case of a solid species. The fluxes $\mathcal{F}_i(z, t)$ consist of several components:

- $\mathcal{F}_{D,i}(z, t)$: the molecular diffusive flux (only for dissolved species) is given by the Fick's law

$$\mathcal{F}_{D,i}(z, t) = -D_i(z, t)\varphi(z) \frac{\partial C_i(z, t)}{\partial z} \quad (\text{S2})$$

- 10 where $D_i(z, t)$ is the effective diffusion coefficient. D_i is usually modelled as a time-independent variable and considered constant for each species at a given salinity and temperature and locally only affected by sediment tortuosity $\theta(z)$. The relation between diffusion coefficient and salinity and temperature is provided in Table S5. Tortuosity has been considered strictly linked to porosity $\varphi(z)$ according to $\theta(z) = 1 - \ln \varphi^2(z)$. And porosity follows an exponential decay with depth (Athy, 1930):

$$15 \quad \varphi(z) = \varphi_0 e^{-c_0 z} \quad (\text{S3})$$

with φ_0 porosity at the Sediment-Water Interface (SWI) and c_0 typical length scale for compaction (Table S5).

- $\mathcal{F}_{D_b,i}(z, t)$: the bioturbation flux, described as a diffusive flux (to be considered also for solid species), reads

$$\mathcal{F}_{D_b,i}(z, t) = -D_{b,i}(z, t)\xi(z) \frac{\partial C_i(z, t)}{\partial z} \quad (\text{S4})$$

- 20 with $D_b(z, t)$ bioturbation coefficient. Considering no time dependency, the latter is assumed to follow an exponential trend below 5 cm depth, *i.e.* :

$$\begin{cases} D_b(z) = D_b^0, & 0 \leq z \leq 5 \text{ cm} \\ D_b(z) = D_b^0 e^{-(z-5)}, & 5 < z < 300 \text{ cm} \end{cases} \quad (\text{S5})$$

and D_b^0 given in Table S5.

- $\mathcal{F}_{v,i}(z,t)$: the advective flux is given by

$$\mathcal{F}_{v,i}(z,t) = v(z,t)\xi(z)C_i(z,t) \quad (\text{S6})$$

where $v(z,t)$ is the sedimentation rate $v(z,t) = \omega(z,t)$ for solid species and the sum of sedimentation rate and possible advective flow velocity $v_{up}(z,t)$ for dissolved species, *i.e.* $v(z,t) = \omega(z,t) + v_{up}(z,t)$. If we assume steady state compaction then burial velocity reads (Berner (1980)):

$$\omega(z) = \left(\frac{1 - \varphi_0}{1 - \varphi(z)} \right) \omega_0 \quad (\text{S7})$$

with ω_0 sedimentation rate at the SWI. A site where $v_{up} \neq 0$ is denominated as *active* while a site with null upward water velocity is defined as *passive*.

- $\mathcal{F}_{NL,i}(z,t)$ represent any form of non-local transport. In its more classical form (Boudreau (1997)) it is given by bioirrigation provided by irrigated furrows digged by benthic fauna and it reads

$$\mathcal{F}_{irr}(z,t) = - \int_0^z \alpha_i(y)\xi(y)[C_i(0,t) - C_i(y,t)]dy \quad (\text{S8})$$

where $\alpha_i(z)$ is the bioirrigation coefficient, $C_i(0,t)$ is the concentration of the species i at the SWI. Bioirrigation parameter α is modelled as (Thullner et al. (2009)):

$$\alpha(z) = \alpha_0 e^{-z/z_{irr}} \quad (\text{S9})$$

where α_0 is the bioirrigation coefficient and z_{irr} the bioirrigation attenuation depth (see Table S5). Yet other forms of non-local transport may be considered in the Arctic shelf scenario, such as ice scouring or bubble migration in sediments rich of free gas. These processes are even more difficult to be modelled and are not included in current BRNS version.

With the fluxes described above eq. S1 takes the form of the standard advection-diffusion-reaction equation (see eq. 4) usually implemented in reactive-transport diagenetic models (Berner (1980); Boudreau (1997))

$$\frac{\partial \xi C_i}{\partial t} = \frac{\partial}{\partial z} \left[(D_i + D_{b,i})\xi \frac{\partial C_i}{\partial z} \right] - \frac{\partial}{\partial z} (v\xi C_i) + \alpha_i \xi (C_i(0) - C_i) + \mathcal{S}_i.$$

S2 Primary redox reactions

Organic matter (OM) decomposition is a complex multi-step process (Arndt et al. (2013)) carried out by micro-organism along a chain of enzyme-mediated biochemical redox reactions which exploits electronic cascades to provide energy. Carbon in organic matter plays the role of electron donor, getting oxidized, and energy yield of the full redox reaction ultimately depends on the terminal electron acceptor (TEA) which overall acts as an oxidant, getting reduced. This entails a preferential sequence

of how OM gets mineralized by microorganism along different metabolic pathways with different TEAs according to energy gain ladder.

It determines the typical vertical zonation of the TEAs and byproducts of organic matter decomposition throughout the sediment column according to the redox sequence (Claypool and Kaplan (1974); Froelich et al. (1979); Stumm and Morgan (1996)). The chained reactions involving OM mineralization are reported in Table S2. OM degradation is modeled by a generalized first order kinetic equation, namely decomposition rate is faster the more OM is present. The proportionality between organic carbon decay rate and organic carbon content is set by a degradability rate k which not necessarily has to be constant. We employed reactive continuum model (RCM) to model this degradability rate k as a continuous variable, whose distribution reads:

$$10 \quad g(k) = \frac{g_0 k^{\nu-1} e^{-ak}}{\Gamma(\nu)} \quad (\text{S10})$$

where g_0 is a scale parameter, ν and a determine the shape of the distribution of k and $\Gamma(\nu)$ is the Gamma function. The quantity a represents the average lifetime of the more reactive organic matter components in a reactive-continuum model (Boudreau and Ruddick (1991)) and the mean degradation constant \bar{k} of the OM spectrum is given by $\bar{k} = \nu/a$. The choice of RCM relies on the fact that it is considered more suitable for marine sediments than a discrete model (Aller and Blair (2004); 15 Arndt et al. (2013)). It manages to encompass all the information about OM degradability in only two parameters, carriers of a theoretical meanings, instead that in as many degradation constants as carbon pools considered in a discrete model. Moreover RCM is more flexible to account for the whole range of degradability that Arctic OM shows, shifting its peak just by tweaking the parameters instead of the initial carbon content of each pool. Another peculiarity of this formulation of RCM is that, assuming distribution in eq. (S10), OM degradation can actually be rewritten as a first-order kinetic with the a degradability 20 $K(t)$ dependent on sediment age t (Boudreau and Ruddick (1991)), *i.e.*

$$\mathcal{S}_{POC} = \frac{dPOC(t)}{dt} = -K(t)POC(t) = -\frac{\nu}{a+t} POC(t) \quad (\text{S11})$$

where $POC(t)$ is the particulate organic carbon, which in turns reads

$$POC(t) = POC(0) \left(\frac{a}{a+t} \right)^\nu \quad (\text{S12})$$

$POC(0)$ being the initial organic carbon concentration. This features allows to estimate sediment age and POC vertical profile 25 just coupling RCM and a discrete model

S3 Estimate of sediment age t and POC content

POC age and vertical profile are critical quantity to be evaluated. One approach would be performing *ab initio* simulations, but they are difficult since a complete knowledge of past boundary conditions and how they evolved over time would be needed. Even when this knowledge is enough, simulation times are usually rather long and hence a different approach is generally used.

Using eq. (S7 and S3), in an unperturbed sediment setting, we find that the age at a certain depth z is provided by

$$t(z) = \int_0^z \frac{1}{\omega(z)} = \frac{z + \frac{\varphi_0}{c_0} (e^{-c_0 z} - 1)}{\omega_0 (1 - \varphi_0)}. \quad (\text{S13})$$

If another formulation for the porosity is employed, for instance:

$$\varphi(z) = \varphi_\infty + (\varphi_0 - \varphi_\infty) e^{-c_0 z} \quad (\text{S14})$$

5 where φ_∞ specifies the asymptotic value of the porosity, then the expression for the age $t(z)$ modifies as:

$$t(z) = \int_0^z \frac{1}{\omega(z)} = \frac{(1 - \varphi_\infty)z + \frac{\varphi_0 - \varphi_\infty}{c_0} (e^{-c_0 z} - 1)}{\omega_0 (1 - \varphi_0)}. \quad (\text{S15})$$

If the sediment column were not bioturbated, plugging results (S13) into eq. (S12) would give the steady state profile of the organic matter throughout the whole sediments, with $POC(0)$ POC concentration at the SWI (because considerations above legitimize a *space for time* substitution and initial time corresponds to the uppermost concentration).

10 The column is instead divided in bioturbated (the upper part) and not-bioturbated (below a certain depth). Because of bioturbation the upper layers are mixed, *i.e.* POC of different ages coexist at the same depth (Meile and Van Cappellen (2005)). This is actually the most difficult problem to be tackled to assign age to a certain sediment level. In order to deal with issue, similarly to **Dale et al 2015**, the POC in the bioturbated zone was modelled resorting to multi-G approximation of the RCM. It means that, within the bioturbated region, the POC is represented by 500 distinct OM fractions, whose reactivity covers 15 the spectrum $k = [k_{min} : 10^{-15}, k_{max} : -\log(a) + 2] \text{ yr}^{-1}$ plus two extra fractions accounting for the reactivity $[0, k_{min}]$ and $[k_{max}, \infty]$. With these considerations and considering constant porosity and sedimentation rate eq. (??) reads:

$$\varphi_s \frac{\partial POC(z, t)}{\partial t} = D_b \varphi_s \frac{\partial^2 POC(z, t)}{\partial z^2} - \omega \varphi_s \frac{\partial POC(z, t)}{\partial z} - \varphi_s k_i POC(z, t) \quad (\text{S16})$$

where $\varphi_s = 1 - \varphi$ and k_i is the reactivity of the i -th fraction of POC considered. Eq. (S16) is an advective-diffusive-reactive equation which in steady state can be analytically solved for each fraction i , once boundary conditions are provided. The 20 general solution is:

$$POC(z) = A e^{\lambda_1 z} + B e^{\lambda_2 z} \quad \text{where} \quad \begin{cases} \lambda_1 = \frac{\omega - \sqrt{\omega^2 + 4D_b k_i}}{2D_b} \\ \lambda_2 = \frac{\omega + \sqrt{\omega^2 + 4D_b k_i}}{2D_b}. \end{cases} \quad (\text{S17})$$

In this case boundary conditions are given by

$$\begin{cases} POC(0) = POC_0 \cdot F_i & \text{at } z = 0 \\ D_b \frac{\partial POC}{\partial z} = 0 & \text{at } z = z_{bio} \end{cases} \quad (\text{S18})$$

where F_i is the fraction of initial POC_0 whose reactivity lies around k_i and z_{bio} is the depth of bioturbated zone where we 25 impose that bioturbated flux shall be null. Bearing in mind eq. (S11) and (S12), the distribution of the POC_0 lying around a

certain value of $k = k_i$ can be written as:

$$f(k_i) = \frac{g(k_i)}{POC_0} = \frac{a^\nu k_i^{\nu-1} e^{-ak_i}}{\Gamma(\nu)}. \quad (\text{S19})$$

The initial fraction of POC_0 whose reactivity is within $[0, k_i]$, i.e. $F(k_i)$, can be obtained via integration of eq. (S19) and this allows to find finally the fraction F_i of POC_0 whose reactivity is in $[k_{i-1}, k_i]$ as

$$5 \quad F_i = F(k_i) - F(k_{i-1}). \quad (\text{S20})$$

Enforcing boundary conditions (S18) for each of 502 fractions and summing up their solutions we find an approximate solution of the RCM in the bioturbated layer. A comparison between the solution obtained in this way and what should be the RCM solution (eq. (S12)) allows to find the apparent age $t(z)$ of the sediments at each depth within the bioturbated zone and also at its bottom, i.e. $t(z_{bio})$. Below the bioturbated zone the apparent age is then found simply adding $t(z_{bio})$ and results of eq. 10 (S13).

The age profile and the POC profile found in this way is then calculated from BRNS at the very beginning and imposed throughout the whole steady-state simulation.

S4 Biogeochemical network: tables

Table S1. The 6 inhibition factors ruling the onset of metabolic pathways according to the succession of the redox ladder.

| | |
|-----------------|---|
| f_{O_2} | $\begin{cases} 1 & \text{if } [O_2] > K_{O_2} \\ \frac{[O_2]}{K_{O_2}} & \text{if } [O_2] < K_{O_2} \end{cases}$ |
| $f_{NO_3^-}$ | $\begin{cases} 0 & \text{if } [O_2] > K_{O_2} \\ \left(1 - \frac{[O_2]}{K_{O_2}}\right) \frac{NO_3^-}{K_{NO_3^-}} & \text{if } [O_2] < K_{O_2} \end{cases}$ |
| f_{MnO_2} | $\begin{cases} 0 & \text{if } [NO_3^-] > K_{NO_3^-} \\ \left(1 - \frac{[O_2]}{K_{O_2}} - \frac{[NO_3^-]}{K_{NO_3^-}}\right) \frac{MnO_2}{K_{MnO_2}} & \text{if } [NO_3^-] < K_{NO_3^-} \end{cases}$ |
| $f_{Fe(OH)_3}$ | $\begin{cases} 0 & \text{if } [MnO_2] > K_{MnO_2} \\ \left(1 - \frac{[O_2]}{K_{O_2}} - \frac{[NO_3^-]}{K_{NO_3^-}} - \frac{[MnO_2]}{K_{MnO_2}}\right) \frac{Fe(OH)_3}{K_{Fe(OH)_3}} & \text{if } [MnO_2] < K_{MnO_2} \end{cases}$ |
| $f_{SO_4^{2-}}$ | $\begin{cases} 0 & \text{if } [Fe(OH)_3] > K_{Fe(OH)_3} \\ \left(1 - \frac{[O_2]}{K_{O_2}} - \frac{[NO_3^-]}{K_{NO_3^-}} - \frac{[MnO_2]}{K_{MnO_2}} - \frac{[Fe(OH)_3]}{K_{Fe(OH)_3}}\right) \frac{SO_4^{2-}}{K_{SO_4^{2-}}} & \text{if } [Fe(OH)_3] < K_{Fe(OH)_3} \end{cases}$ |
| f_{CH_4} | $\begin{cases} 0 & \text{if } [SO_4^{2-}] > K_{SO_4^{2-}} \\ \left(1 - \frac{[O_2]}{K_{O_2}} - \frac{[NO_3^-]}{K_{NO_3^-}} - \frac{[MnO_2]}{K_{MnO_2}} - \frac{[Fe(OH)_3]}{K_{Fe(OH)_3}} - \frac{[SO_4^{2-}]}{K_{SO_4^{2-}}}\right) \frac{CH_4}{K_{CH_4}} & \text{if } [SO_4^{2-}] < K_{SO_4^{2-}} \end{cases}$ |

Table S2. The 6 primary redox reactions involved in the degradation of OM. The coefficients x , y and z , enforce Redfield ratio ($x = 106$, $y = 16$ and $z = 1$). SD stands for the conversion factor between solid and liquid volume, i.e. $SD = \varphi_s/\varphi$. For the expression of the inhibition factors f see Table S1. $[\text{CH}_2\text{O}]$ is a shortcut for $(\text{CH}_2\text{O})(\text{NH}_3)^{\frac{y}{x}}(\text{H}_3\text{PO}_4)^{\frac{z}{x}}$, to take into account nutrients.

| # | Reaction | Rate expression |
|----|---|--|
| R1 | $[\text{CH}_2\text{O}] + (\frac{x+2y}{x}) SD \cdot \text{O}_2 + (\frac{y+2z}{x}) SD \cdot \text{HCO}_3^- \longrightarrow (\frac{x+y+2z}{x}) SD \cdot \text{CO}_2 + (\frac{y}{x}) SD \cdot \text{NO}_3^- + (\frac{z}{x}) SD \cdot \text{HPO}_4^{2-} + (\frac{x+2y+2z}{x}) SD \cdot \text{H}_2\text{O}$ | $\frac{\nu}{a+t} [\text{CH}_2\text{O}] \cdot f_{\text{O}_2}$ |
| R2 | $[\text{CH}_2\text{O}] + (\frac{4x+3y}{5x}) SD \cdot \text{NO}_3^- \longrightarrow (\frac{x-3y+10z}{5x}) SD \cdot \text{CO}_2 + (\frac{4x+3y-10z}{5x}) SD \cdot \text{HCO}_3^- + (\frac{z}{x}) SD \cdot \text{HPO}_4^{2-} + (\frac{3x+6y+10z}{5x}) \text{H}_2\text{O} + (\frac{2x+4y}{5x}) \text{N}_2$ | $\frac{\nu}{a+t} [\text{CH}_2\text{O}] \cdot f_{\text{NO}_3^-}$ |
| R3 | $[\text{CH}_2\text{O}] + 2\text{MnO}_2 + (\frac{3x+y-2z}{x}) SD \cdot \text{CO}_2 + (\frac{x+y-2z}{x}) SD \cdot \text{H}_2\text{O} \longrightarrow 2SD \cdot \text{Mn}^{2+} + (\frac{y}{x}) SD \cdot \text{NH}_4^+ + (\frac{4x+y-2z}{x}) SD \cdot \text{HCO}_3^- + (\frac{z}{x}) SD \cdot \text{HPO}_4^{2-}$ | $\frac{\nu}{a+t} \cdot [\text{CH}_2\text{O}] \cdot f_{\text{MnO}_2}$ |
| R4 | $[\text{CH}_2\text{O}] + 4\text{Fe(OH)}_3 + (\frac{7x+y-2z}{x}) SD \cdot \text{CO}_2 \longrightarrow 4\text{SD} \cdot \text{Fe}^{2+} + (\frac{8x+y-2z}{x}) SD \cdot \text{HCO}_3^- + (\frac{y}{x}) SD \cdot \text{NH}_4^+ + (\frac{z}{x}) SD \cdot \text{HPO}_4^{2-} + (\frac{3x-y+2z}{x}) \text{H}_2\text{O}$ | $\frac{\nu}{a+t} \cdot [\text{CH}_2\text{O}] \cdot f_{\text{Fe(OH)}_3}$ |
| R5 | $[\text{CH}_2\text{O}] + \frac{1}{2}\text{SD} \cdot \text{SO}_4^{2-} + (\frac{y-2z}{x}) SD \cdot \text{CO}_2 + (\frac{y-2z}{x}) SD \cdot \text{H}_2\text{O} \longrightarrow (\frac{x+y-2z}{x}) SD \cdot \text{HCO}_3^- + (\frac{y}{x}) SD \cdot \text{NH}_4^+ + \frac{1}{2}\text{SD} \cdot \text{H}_2\text{S} + (\frac{z}{x}) SD \cdot \text{HPO}_4^{2-}$ | $\frac{\nu}{a+t} \cdot [\text{CH}_2\text{O}] \cdot f_{\text{SO}_4^{2-}}$ |
| R6 | $[\text{CH}_2\text{O}] \longrightarrow (\frac{x-2y+4z}{2x}) SD \cdot \text{CO}_2 + (\frac{y-2z}{x}) SD \cdot \text{HCO}_3^- + (\frac{y}{x}) SD \cdot \text{NH}_4^+ + \frac{1}{2}\text{SD} \cdot CH4 + (\frac{z}{x}) SD \cdot \text{HPO}_4^{2-}$ | $\frac{\nu}{a+t} \cdot [\text{CH}_2\text{O}] \cdot f_{\text{CH}_4}$ |

Table S3. The secondary redox, precipitation, absorption and equilibrium reactions

| # | Reaction | Rate expression |
|-----|---|---|
| R7 | $2\text{O}_2 + \text{NH}_4^+ + 2\text{HCO}_3^- \longrightarrow \text{NO}_3^- + 2\text{CO}_2 + 3\text{H}_2\text{O}$ | $k_7[\text{O}_2][\text{NH}_4^+]$ |
| R8 | $\frac{1}{2}\text{O}_2 + \text{Mn}^{2+} + 2\text{HCO}_3^- \longrightarrow \frac{\text{MnO}_2}{SD} + 2\text{CO}_2 + \text{H}_2\text{O}$ | $k_8[\text{O}_2][\text{Mn}^{2+}]$ |
| R9 | $\text{MnO}_2 + 2\text{SD} \cdot \text{Fe}^{2+} + 2\text{SD} \cdot \text{HCO}_3^- + 2\text{SD} \cdot \text{H}_2\text{O} \longrightarrow 2\text{Fe(OH)}_3 + \text{SD} \cdot \text{Mn}^{2+} + 2\text{SD} \cdot \text{CO}_2$ | $k_9[\text{Fe}^{2+}][\text{MnO}_2]$ |
| R10 | $\frac{1}{4}\text{O}_2 + \text{Fe}^{2+} + 2\text{HCO}_3^- + \frac{1}{2}\text{H}_2\text{O} \longrightarrow \frac{\text{Fe(OH)}_3}{SD} + 2\text{CO}_2$ | $k_{10}[\text{O}_2][\text{Fe}^{2+}]$ |
| R11 | $2\text{O}_2 + \text{H}_2\text{S} + 2\text{HCO}_3^- \longrightarrow \text{SO}_4^{2-} + 2\text{CO}_2 + 2\text{H}_2\text{O}$ | $k_{11}[\text{O}_2](\text{H}_2\text{S} + [\text{HS}^-])$ |
| R12 | $\text{MnO}_2 + \text{SD} \cdot \text{H}_2\text{S} + 2\text{SD} \cdot \text{CO}_2 \longrightarrow \text{S}^0 + \text{SD} \cdot \text{Mn}^{2+} + 2\text{SD} \cdot \text{HCO}_3^-$ | $k_{12}[\text{MnO}_2](\text{H}_2\text{S} + [\text{HS}^-])$ |
| R13 | $2\text{Fe(OH)}_3 + \text{SD} \cdot \text{H}_2\text{S} + 4\text{SD} \cdot \text{CO}_2 \longrightarrow \text{S}^0 + 2\text{SD} \cdot \text{Fe}^{2+} + 4\text{SD} \cdot \text{HCO}_3^-$ | $k_{13}[\text{Fe(OH)}_3](\text{H}_2\text{S} + [\text{HS}^-])$ |
| R14 | $\text{CH}_4 + 2\text{O}_2 \longrightarrow \text{CO}_2 + 2\text{H}_2\text{O}$ | $k_{14}[\text{CH}_4][\text{O}_2]$ |
| R15 | $\text{FeS} + \text{SD} \cdot \text{O}_2 \longrightarrow \text{S}^0 + \text{SD} \cdot \text{Fe}^{2+} + \text{SD} \cdot \text{SO}_4^{2-}$ | $k_{15}[\text{FeS}][\text{O}_2]$ |
| R16 | $\text{Mn}^{2+} + 2\text{HCO}_3^- \longrightarrow \frac{\text{MnCO}_3}{SD} + \text{CO}_2 + \text{H}_2\text{O}$ | $\begin{cases} k_{16} \left(\frac{[\text{Mn}^{2+}][\text{CO}_3^{2-}]}{K_s \text{MnCO}_3} - 1 \right) & \text{if } [\text{Mn}^{2+}][\text{CO}_3^{2-}] > K_s \text{MnCO}_3 \\ 0 & \text{if } [\text{Mn}^{2+}][\text{CO}_3^{2-}] < K_s \text{MnCO}_3 \end{cases}$ |
| R17 | $\text{Fe}^{2+} + \text{H}_2\text{S} + 2\text{HCO}_3^- \longrightarrow \frac{\text{FeS}}{SD} + 2\text{CO}_2 + 2\text{H}_2\text{O}$ | $\begin{cases} k_{17} \left(\frac{[\text{Fe}^{2+}][\text{HS}^-]}{[\text{H}^+]K_s \text{FeS}} - 1 \right) & \text{if } \frac{[\text{Fe}^{2+}][\text{HS}^-]}{[\text{H}^+]K_s \text{FeS}} > K_s \text{FeS} \\ 0 & \text{if } \frac{[\text{Fe}^{2+}][\text{HS}^-]}{[\text{H}^+]K_s \text{FeS}} < K_s \text{FeS} \end{cases}$ |

| | | |
|-----|---|---|
| R18 | $\frac{FeS}{SD} + 2CO_2 + 2H_2O \longrightarrow Fe^{2+} + H_2S + 2HCO_3^-$ | $\begin{cases} k_{18} \left(1 - \frac{[Fe^{2+}][HS^-]}{[H^+][K_s FeS]} \right) & \text{if } \frac{[Fe^{2+}][HS^-]}{[H^+]} < K_s FeS \\ 0 & \text{if } \frac{[Fe^{2+}][HS^-]}{[H^+]} > K_s FeS \end{cases}$ |
| R19 | $Fe^{2+} + 2HCO_3^- \longrightarrow FeCO_3 + CO_2 + H_2O$ | $\begin{cases} k_{19} \left(\frac{[Fe^{2+}][CO_3^{2-}]}{K_{sFeCO_3}} - 1 \right) & \text{if } [Fe^{2+}][CO_3^{2-}] > K_{sFeCO_3} \\ 0 & \text{if } [Fe^{2+}][CO_3^{2-}] < K_{sFeCO_3} \end{cases}$ |
| R20 | $FeS + SD \cdot H_2S \longrightarrow FeS_2$ | $k_{20} [FeS] ([H_2S] + [HS^-])$ |
| R21 | $3FeS + SD \cdot S^0 \longrightarrow Fe_3S_4$ | $k_{21} [FeS] [S^0]$ |
| R22 | $PO_4^{3-} \longrightarrow CFA$ | $\begin{cases} k_{22} ([PO_4^{3-}] - [PO_4^{3-}]) & \text{if } [PO_4^{3-}] > [PO_4^{3-}]^* \\ 0 & \text{if } [PO_4^{3-}] < [PO_4^{3-}]^* \end{cases}$ |
| R23 | $CaCO_3 + SD \cdot H^+ \longrightarrow SD \cdot Ca^{2+} + SD \cdot HCO_3^-$ | $\begin{cases} k_{23} \left(1 - \frac{[Ca^{2+}][CO_3^{2-}]}{K_{sCaCO_3}} \right) & \text{if } [Ca^{2+}][CO_3^{2-}] < K_{sCaCO_3} \\ 0 & \text{if } [Ca^{2+}][CO_3^{2-}] > K_{sCaCO_3} \end{cases}$ |
| R24 | $Ca^{2+} + HCO_3^- \longrightarrow \frac{CaCO_3}{SD} + H^+$ | $\begin{cases} k_{24} \left(\frac{[Ca^{2+}][CO_3^{2-}]}{K_{sCaCO_3}} - 4.5 \right) & \text{if } [Ca^{2+}][CO_3^{2-}] > 4.5 \\ 0 & \text{if } [Ca^{2+}][CO_3^{2-}] < 4.5 \end{cases}$ |
| R25 | $CH_4(g) \longrightarrow CH_4(aq)$ | $\begin{cases} k_{25} [CH_4(g)] ([CH_4]^* - [CH_4]) & \text{if } [CH_4] < [CH_4]^* \\ 0 & \text{if } [CH_4] > [CH_4]^* \end{cases}$ |
| R26 | $CH_4(aq) \longrightarrow CH_4(g)$ | $\begin{cases} k_{26} ([CH_4] - [CH_4]^*) & \text{if } [CH_4] > [CH_4]^* \\ 0 & \text{if } [CH_4] < [CH_4]^* \end{cases}$ |
| R27 | $4S^0 + 4H_2O \longrightarrow SO_4^{2-} + 3H_2S + 2H^+$ | $k_{27} [S^0]$ |
| R28 | $NH_4^+(aq) \longrightarrow NH_4^+(ads)$ | $k_{28}^f [NH_4^+(aq)] \varphi - k_{28}^b [NH_4^+(ads)] \varphi_s$ |
| R29 | $PO_4^{3-}(aq) \longrightarrow PO_4^{3-}(ads)$ | $k_{29}^f [PO_4^{3-}(aq)] \varphi - k_{29}^b [PO_4^{3-}(ads)] \varphi_s$ |
| R30 | $Fe^{2+}(aq) \longrightarrow Fe^{2+}(ads)$ | $k_{30}^f [Fe^{2+}(aq)] \varphi - k_{30}^b [Fe^{2+}(ads)] \varphi_s$ |

| | | |
|-----|---|---|
| R31 | $\text{FeOH}_3 + \text{PO}_4^{3-} \longrightarrow \text{PO}_4(\text{ads}_{\text{Fe(OH)3}})$ | $k_{31}^f[\text{PO}_4^{3-}][\text{Fe}(\text{OH})_3] - k_{31}^b[\text{PO}_4(\text{ads}_{\text{Fe(OH)3}})]$ |
| R32 | $\text{CO}_2 + \text{H}_2\text{O} \longrightarrow \text{H}^+ + \text{HCO}_3^-$ | k_{32} thermodynamic equilibrium |
| R33 | $\text{HCO}_3^- \longrightarrow \text{H}^+ + \text{CO}_3^{2-}$ | k_{33} thermodynamic equilibrium |
| R34 | $\text{H}_2\text{S} \longrightarrow \text{H}^+ + \text{HS}^-$ | k_{34} thermodynamic equilibrium |
| R35 | $\text{B}(\text{OH})_3 \longrightarrow \text{B}(\text{OH})_4^- + \text{H}^+$ | k_{35} thermodynamic equilibrium |

S5 Model validations

S5.1 Sediment core offshore Vesterålen Archipelago

Table S4. Model boundary parameters and boundary conditions for the case study of a cold seep off Vesterålen, Norway. Values with * are set for this study. All the other variables are as in Sauer et al. (2015, 2016). $[]_-$ stands for lower boundary conditions, while $[]_+$ stand for upper boundary conditions.

| Quantity | Value | Units |
|------------------------|-------|---------------------|
| a^* | 1100 | yr |
| ν^* | 100 | - |
| v_{up} | 0 | cm yr^{-1} |
| C/N^* | 14.8 | - |
| $[\text{SO}_4^{2-}]_+$ | 28.3 | mM |
| $[\text{SO}_4^{2-}]_-$ | 0.0 | mM |
| $[\text{CH}_4]_+$ | 42 | nM |
| $[\text{CH}_4]_-^*$ | 35 | mM |
| $[\text{NH}_4^+]_+$ | 9.1 | μM |
| $[\text{NH}_4^+]_-$ | 0.227 | mM |

S6 Sensitivity study: model parameters and model boundary conditions. Tables

Table S5. Generic model parameters. The parameters below the red line at the bottom are the quantities involved in the bioenergetic formulation of AOM. Diffusion coefficients depends on temperature $T(^{\circ}\text{C})$, salinity S and porosity φ according to the relation

$$D(T, S, \varphi) = \frac{D(1 + \mu T(^{\circ}\text{C}))}{1 - \ln(\varphi^2)}.$$

| Quantity | Value | Units | Reference |
|-----------|---------------------|------------------------------|--------------------------|
| ν | 0.125 | - | This study |
| SD | φ_s/φ | - | Athy (1930) |
| S | 20 | psu | This study |
| ρ | 2.41 | g cm^{-3} | Berg (2003) |
| D_b^0 | 29.8 | $\text{cm}^2 \text{yr}^{-1}$ | Middelburg et al. (1997) |
| z_{bio} | 5 | $\text{cm}^2 \text{yr}^{-1}$ | Boudreau (1997) |
| z_{irr} | 3.5 | cm | Thullner et al. (2009) |

| | | | |
|----------------------------------|---------------------|--|-------------------------------|
| T | 0, 273.15 | °C, K | This study |
| C:N | 106:16 | - | Redfield ratio |
| C:P | 106:1 | - | Redfield ratio |
| D_{O_2}, μ_{O_2} | 380.45, 0.06 | $\text{cm}^2 \text{ yr}^{-1}, T^{-1}$ | Dale et al. (2012) |
| $D_{NO_3^-}, \mu_{NO_3^-}$ | 394.59, 0.038 | $\text{cm}^2 \text{ yr}^{-1}, T^{-1}$ | Van Cappellen and Wang (1996) |
| $D_{SO_4^{2-}}, \mu_{SO_4^{2-}}$ | 173.92, 0.045 | $\text{cm}^2 \text{ yr}^{-1}, T^{-1}$ | Dale et al. (2012) |
| D_{CH_4}, μ_{CH_4} | 263.94, 0.052 | $\text{cm}^2 \text{ yr}^{-1}, T^{-1}$ | Van Cappellen and Wang (1996) |
| $D_{NH_4^+}, \mu_{NH_4^+}$ | 395.87, 0.041 | $\text{cm}^2 \text{ yr}^{-1}, T^{-1}$ | Van Cappellen and Wang (1996) |
| $D_{PO_4^{3-}}, \mu_{PO_4^{3-}}$ | 112.36, 0.054 | $\text{cm}^2 \text{ yr}^{-1}, T^{-1}$ | Van Cappellen and Wang (1996) |
| $D_{Mn^{2+}}, \mu_{Mn^{2+}}$ | 123.39, 0.05 | $\text{cm}^2 \text{ yr}^{-1}, T^{-1}$ | Van Cappellen and Wang (1996) |
| $D_{Fe^{2+}}, \mu_{Fe^{2+}}$ | 136.24, 0.044 | $\text{cm}^2 \text{ yr}^{-1}, T^{-1}$ | Dale et al. (2012) |
| D_{H_2S}, μ_{H_2S} | 331.61, 0.06 | $\text{cm}^2 \text{ yr}^{-1}, T^{-1}$ | Van Cappellen and Wang (1996) |
| D_{HS^-}, μ_{HS^-} | 392.02, 0.031 | $\text{cm}^2 \text{ yr}^{-1}, T^{-1}$ | Van Cappellen and Wang (1996) |
| $D_{CH_4(g)}, \mu_{CH_4(g)}$ | 5000.0, 0.0 | $\text{cm}^2 \text{ yr}^{-1}, T^{-1}$ | Van Cappellen and Wang (1996) |
| $D_{H_2CO_3}, \mu_{H_2CO_3}$ | 320.04, 0.06 | $\text{cm}^2 \text{ yr}^{-1}, T^{-1}$ | Van Cappellen and Wang (1996) |
| $D_{HCO_3^-}, \mu_{HCO_3^-}$ | 217.22, 0.048 | $\text{cm}^2 \text{ yr}^{-1}, T^{-1}$ | Van Cappellen and Wang (1996) |
| $D_{CO_3^{2-}}, \mu_{CO_3^{2-}}$ | 176.09, 0.047 | $\text{cm}^2 \text{ yr}^{-1}, T^{-1}$ | Van Cappellen and Wang (1996) |
| $D_{B(OH)_3}, \mu_{B(OH)_3}$ | 110.05, 0.054 | $\text{cm}^2 \text{ yr}^{-1}, T^{-1}$ | Van Cappellen and Wang (1996) |
| $D_{B(OH)_4^-}, \mu_{B(OH)_4^-}$ | 96.30, 0.041 | $\text{cm}^2 \text{ yr}^{-1}, T^{-1}$ | Van Cappellen and Wang (1996) |
| D_{H^+}, μ_{H^+} | 600.0, 0.05 | $\text{cm}^2 \text{ yr}^{-1}, T^{-1}$ | Van Cappellen and Wang (1996) |
| $D_{Ca^{2+}}, \mu_{Ca^{2+}}$ | 150.38, 0.045 | $\text{cm}^2 \text{ yr}^{-1}, T^{-1}$ | Van Cappellen and Wang (1996) |
| D_{S^0}, μ_{S^0} | 173.92, 0.045 | $\text{cm}^2 \text{ yr}^{-1}, T^{-1}$ | Van Cappellen and Wang (1996) |
| φ_0 | 0.45 | - | LaRowe et al. (2017) |
| c_0 | $0.5 \cdot 10^{-3}$ | m^{-1} | LaRowe et al. (2017) |
| φ_∞ | 0.35 | - | This study |
| K_{O_2} | 8 | μM | Thullner et al. (2009) |
| $K_{NO_3^-}$ | 5 | μM | Van Cappellen and Wang (1996) |
| K_{MnO_2} | 2 | $\mu\text{mol/g}_d$ | Thullner et al. (2009) |
| $K_{Fe(OH)_3}$ | 5 | $\mu\text{mol/g}_d$ | Thullner et al. (2009) |
| $K_{SO_4^{2-}}$ | 100 | μM | Dale et al. (2006) |
| k_7 | $1.0 \cdot 10^7$ | $\text{cm}^3 \text{ mol}^{-1} \text{ yr}^{-1}$ | Van Cappellen and Wang (1996) |
| k_8 | $2.0 \cdot 10^9$ | $\text{M}^{-1} \text{ yr}^{-1}$ | Thullner et al. (2009) |
| k_9 | $2.0 \cdot 10^8$ | $\text{M}^{-1} \text{ yr}^{-1}$ | Thullner et al. (2009) |

| | | | |
|------------------------|------------------------|--|-------------------------------|
| k_{10} | $1.0 \cdot 10^{11}$ | $\text{cm}^3 \text{ mol}^{-1} \text{ yr}^{-1}$ | Van Cappellen and Wang (1996) |
| k_{11} | $1.0 \cdot 10^9$ | $\text{cm}^3 \text{ mol}^{-1} \text{ yr}^{-1}$ | Van Cappellen and Wang (1996) |
| k_{12} | $1.0 \cdot 10^4$ | $\text{M}^{-1} \text{ yr}^{-1}$ | Thullner et al. (2009) |
| k_{13} | $1.0 \cdot 10^4$ | $\text{M}^{-1} \text{ yr}^{-1}$ | Thullner et al. (2009) |
| k_{14} | $1.0 \cdot 10^{13}$ | $\text{cm}^3 \text{ mol}^{-1} \text{ yr}^{-1}$ | Van Cappellen and Wang (1996) |
| k_{15} | $1.0 \cdot 10^9$ | $\text{cm}^3 \text{ mol}^{-1} \text{ yr}^{-1}$ | Van Cappellen and Wang (1996) |
| k_{16} | $1.0 \cdot 10^{-8}$ | $\text{mol cm}^{-3} \text{ yr}^{-1}$ | Van Cappellen and Wang (1996) |
| k_{17} | $5 \cdot 10^{-9}$ | $\text{mol cm}^{-3} \text{ yr}^{-1}$ | Van Cappellen and Wang (1996) |
| k_{18} | $1.0 \cdot 10^{-3}$ | $\text{mol cm}^{-3} \text{ yr}^{-1}$ | Van Cappellen and Wang (1996) |
| k_{19} | $1.0 \cdot 10^{-9}$ | $\text{mol cm}^{-3} \text{ yr}^{-1}$ | Van Cappellen and Wang (1996) |
| k_{20} | $6.0 \cdot 10^7$ | $\text{cm}^3 \text{ mol}^{-1} \text{ yr}^{-1}$ | Van Cappellen and Wang (1996) |
| k_{21} | $2.4 \cdot 10^4$ | $\text{cm}^3 \text{ mol}^{-1} \text{ yr}^{-1}$ | Van Cappellen and Wang (1996) |
| k_{22} | 1 | yr^{-1} | Van Cappellen and Wang (1996) |
| k_{23} | 0.1 | $\text{mol cm}^{-3} \text{ yr}^{-1}$ | Van Cappellen and Wang (1996) |
| k_{24} | 24.16 | $\text{M}^{-1} \text{ yr}^{-1}$ | Wallmann et al. (2006) |
| k_{25} | $1.0 \cdot 10^9$ | $\text{cm}^3 \text{ mol}^{-1} \text{ yr}^{-1}$ | Van Cappellen and Wang (1996) |
| k_{26} | $7.89 \cdot 10^2$ | yr^{-1} | Pauss et al. (1990) |
| k_{27} | $1.0 \cdot 10^{-3}$ | yr^{-1} | Van Cappellen and Wang (1996) |
| k_{28}^f | 1.6 | yr^{-1} | Van Cappellen and Wang (1996) |
| k_{28}^b | 1.0 | yr^{-1} | Van Cappellen and Wang (1996) |
| k_{29}^f | 1.8 | yr^{-1} | Van Cappellen and Wang (1996) |
| k_{29}^b | 1.0 | yr^{-1} | Van Cappellen and Wang (1996) |
| k_{30}^f | 400 | yr^{-1} | Van Cappellen and Wang (1996) |
| k_{30}^b | 1.0 | yr^{-1} | Van Cappellen and Wang (1996) |
| k_{31}^f | 100 | yr^{-1} | Van Cappellen and Wang (1996) |
| k_{31}^b | 1.0 | yr^{-1} | Van Cappellen and Wang (1996) |
| k_{32} | $8.470 \cdot 10^{-7}$ | M | Millero (1995) |
| k_{33} | $4.300 \cdot 10^{-10}$ | M | Millero (1995) |
| k_{34} | $1.602 \cdot 10^{-7}$ | M | Millero (1995) |
| k_{35} | $1.318 \cdot 10^{-9}$ | M | Millero (1995) |
| $[\text{CH}_4]^*$ | 5.46 | mM | Dale et al. (2008a) |
| $[\text{PO}_4^{3-}]^*$ | 10 | μM | This study |
| $K_{s\text{MnCO}_3}$ | $3.2 \cdot 10^{-9}$ | M^2 | Van Cappellen and Wang (1996) |

| | | | |
|--------------------------|---------------------|---------------------|-------------------------------|
| $K_{s\text{FeCO}_3}$ | $4.0 \cdot 10^{-9}$ | M^2 | Van Cappellen and Wang (1996) |
| $K_{s\text{FeS}}$ | $8.2 \cdot 10^{-4}$ | M | Van Cappellen and Wang (1996) |
| $K_{s\text{CaCO}_3}$ | $3.8 \cdot 10^{-7}$ | M^2 | Mucci (1983); Millero (1995) |
| μ_g | 18.3 | yr^{-1} | Dale et al. (2006, 2008b) |
| μ_d | 0.1 | yr^{-1} | Dale et al. (2006, 2008b) |
| γ | 2.48 | - | Dale et al. (2006, 2008b) |
| χ | 8.0 | - | Dale et al. (2006, 2008b) |
| ΔG_{BQ} | 20 | kJ/mol e^- | Dale et al. (2006, 2008b) |
| ΔG_r^0 | -29.92 | kJ/mol e^- | Regnier et al. (2011) |
| $K_m^{\text{CH}_4}$ | $1.5 \cdot 10^{-3}$ | M | Dale et al. (2006, 2008b) |
| $K_m^{\text{SO}_4^{2-}}$ | $1.0 \cdot 10^{-3}$ | M | Dale et al. (2006, 2008b) |

Table S6. Generic model upper boundary conditions. The boundary condition for biomass is applied only in the bioenergetic formulation of AOM

| Species | Value @ SWI | Units | Reference |
|-------------------------|-------------|--|-----------------------------------|
| POC | 1.04 | % | This study |
| O_2 | 306.98 | μM | Garcia et al. (2010a) |
| NO_3^- | 11.51 | μM | Garcia et al. (2010b) |
| MnO_2 | 2.18 | $\mu\text{mol cm}^{-2} \text{yr}^{-1}$ | Dale et al. (2015); Glasby (2006) |
| Fe(OH)_3 | 7.09 | $\mu\text{mol cm}^{-2} \text{yr}^{-1}$ | Dale et al. (2015); Glasby (2006) |
| SO_4^{2-} | 28.0 | mM | Thullner et al. (2009) |
| CH_4 | 0.0 | mM | This study |
| NH_4^+ | 0.0 | mM | This study |
| PO_4^{3-} | 1.0 | μM | Sales de Freitas (2018) |
| Mn^{2+} | 1.0 | μM | Sales de Freitas (2018) |
| Fe^{2+} | 1.0 | pM | Sales de Freitas (2018) |
| H_2S | 0.835 | nM | Sales de Freitas (2018) |
| HS^- | 9.17 | nM | Sales de Freitas (2018) |
| $\text{CH}_4(\text{g})$ | 0.0 | nM | This study |
| H_2CO_3 | 39 | μM | Sales de Freitas (2018) |
| HCO_3^- | 2150 | μM | Sales de Freitas (2018) |

| | | | |
|---|------------------------------------|--|-------------------------|
| CO_3^{2-} | 15.3 | μM | Sales de Freitas (2018) |
| B(OH)_3 | 363.6 | μM | Sales de Freitas (2018) |
| B(OH)_4^- | 61.4 | μM | Sales de Freitas (2018) |
| H^+ | 6.31 | μM | Sales de Freitas (2018) |
| CaCO_3 | 23 | $\mu\text{mol cm}^{-2} \text{yr}^{-1}$ | Sales de Freitas (2018) |
| Ca^{2+} | 9.7 | mM | Sales de Freitas (2018) |
| $\text{NH}_4^+(\text{ads})$ | 0 | mM | Sales de Freitas (2018) |
| $\text{PO}_4^{3-}(\text{ads})$ | 0 | mM | Sales de Freitas (2018) |
| FeS | 0 | $\mu\text{mol cm}^{-2} \text{yr}^{-1}$ | Sales de Freitas (2018) |
| FeCO_3 | 0 | mM | Sales de Freitas (2018) |
| S^0 | 0 | mM | Sales de Freitas (2018) |
| FeS_2 | 0 | $\mu\text{mol cm}^{-2} \text{yr}^{-1}$ | Sales de Freitas (2018) |
| $\text{Fe}^{2+}(\text{ads})$ | 0 | mM | Sales de Freitas (2018) |
| $\text{PO}_4(\text{ads}_{\text{Fe(OH)}_3})$ | 0 | Mm | Sales de Freitas (2018) |
| B | $1.0 \cdot 10^8, 3.158 \cdot 10^7$ | $\text{mol cm}^{-3}, \text{cells cm}^{-3}$ | This study |

Table S7. Name, location, water depth and linear sedimentation rate for cores used to inter- and extra-polate the sedimentation rates to the whole Laptev sea area via simple 3D kriging.

| Core name | Lon ($^\circ$) | Lat ($^\circ$) | Water depth (m) | ω (cm/yr) | Reference |
|-------------|------------------|------------------|-----------------|------------------|---------------------|
| KD9502-14 | 133.117 | 76.192 | 46 | 0.003 | Bauch et al. (2001) |
| PM9462-4 | 136.005 | 74.503 | 27 | 0.05 | Bauch et al. (2001) |
| PM9499-2 | 115.545 | 75.501 | 48 | 0.004 | Bauch et al. (2001) |
| PS51/080-13 | 131.638 | 73.459 | 21 | 0.028 | Bauch et al. (2001) |
| PS51/092-13 | 130.136 | 74.594 | 32 | 0.07 | Bauch et al. (2001) |
| PS51/092-12 | 130.138 | 74.593 | 32 | 0.041 | Bauch et al. (2001) |
| PS51/118-2 | 132.237 | 77.892 | 114 | 0.002 | Bauch et al. (2001) |
| PS51/118-3 | 132.199 | 77.892 | 122 | 0.008 | Bauch et al. (2001) |
| PS51/135-4 | 133.243 | 76.165 | 51 | 0.031 | Bauch et al. (2001) |
| PS51/141-2 | 128.641 | 75.227 | 42 | 0.011 | Bauch et al. (2001) |
| PS51/154-11 | 120.610 | 77.276 | 270 | 0.012 | Bauch et al. (2001) |

| | | | | | |
|-------------|---------|--------|------|-------|-----------------------|
| PS51/159-10 | 116.032 | 76.767 | 60 | 0.011 | Bauch et al. (2001) |
| PS2458-4 | 133.398 | 78.167 | 983 | 0.027 | Bauch et al. (2001) |
| L13-09-2 | 129.895 | 73.018 | 10 | 0.45 | Han (2014) |
| L13-14-2 | 130.695 | 73.857 | 25 | 0.16 | Han (2014) |
| L13-18-2 | 130.479 | 73.032 | 16 | 0.3 | Han (2014) |
| L13-04-2 | 130.690 | 71.902 | 15 | 0.2 | Han (2014) |
| C-37 | 130.367 | 71.617 | 10 | 0.024 | Stein and Fahl (2000) |
| C-4 | 131.000 | 73.167 | 26 | 0.17 | Stein and Fahl (2000) |
| C-7 | 129.983 | 74.883 | 37 | 0.159 | Stein and Fahl (2000) |
| C-8 | 130.500 | 75.400 | 48 | 0.015 | Stein and Fahl (2000) |
| C-11 | 130.083 | 76.867 | 66 | 0.011 | Stein and Fahl (2000) |
| PS2725-5 | 144.135 | 78.656 | 77 | 0.013 | Stein et al. (2001) |
| PS2778-2 | 113.065 | 77.978 | 341 | 0.038 | Stein et al. (2001) |
| PS2476-4 | 118.193 | 77.39 | 521 | 0.05 | Stein et al. (2001) |
| PS2742-5 | 103.815 | 80.788 | 1890 | 0.022 | Stein et al. (2001) |
| PS2474-3 | 118.575 | 77.67 | 1494 | 0.02 | Stein et al. (2001) |
| PS2741-1 | 105.395 | 81.105 | 2400 | 0.012 | Stein et al. (2001) |
| PS2471-4 | 119.793 | 79.152 | 3047 | 0.002 | Stein et al. (2001) |

S6.1 Sensitivity study: model parameters and model boundary conditions. Figures

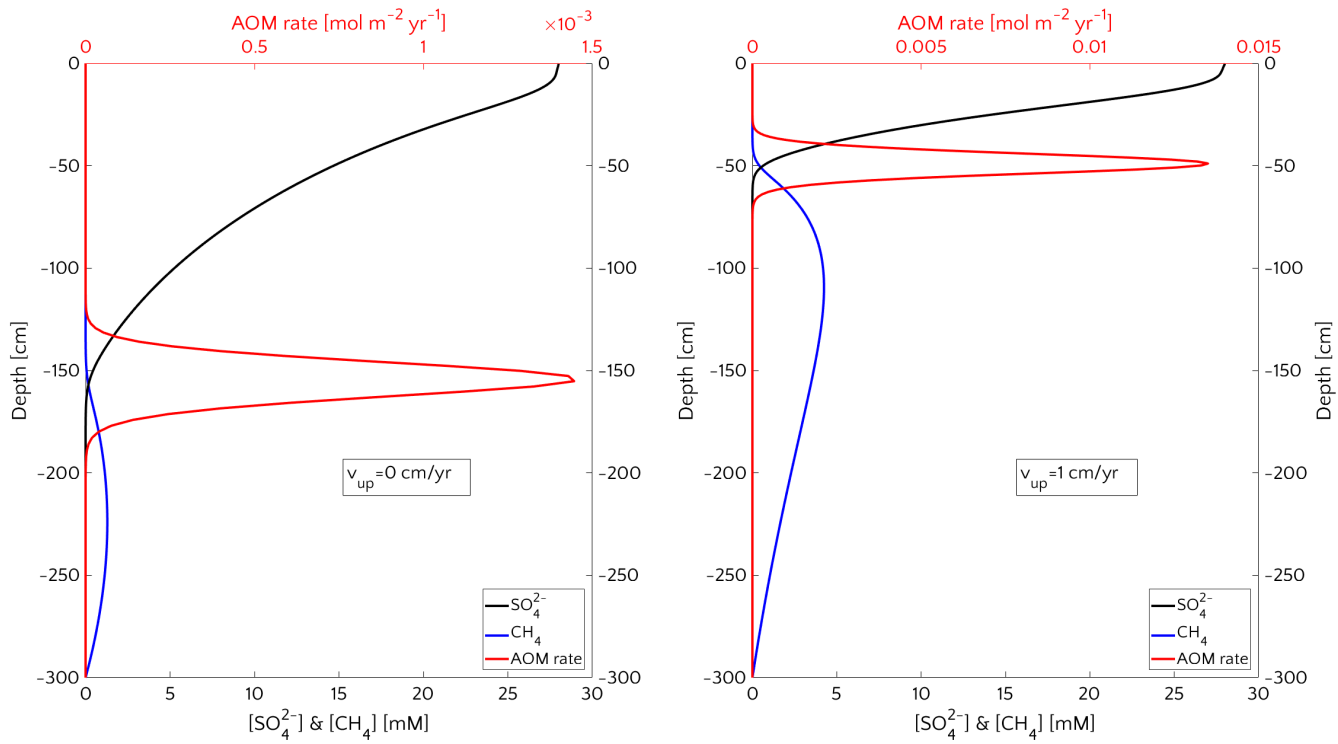


Figure S1. Outcomes for the baseline simulations at steady state. Passive case (left) and active case with $v_{up} = 1 \text{ cm/yr}$ (right). Typical SMTZ shoaling (from 155.2 cm to 48.9 cm) and squeezing (from 65 cm to 38 cm) from passive to active case.

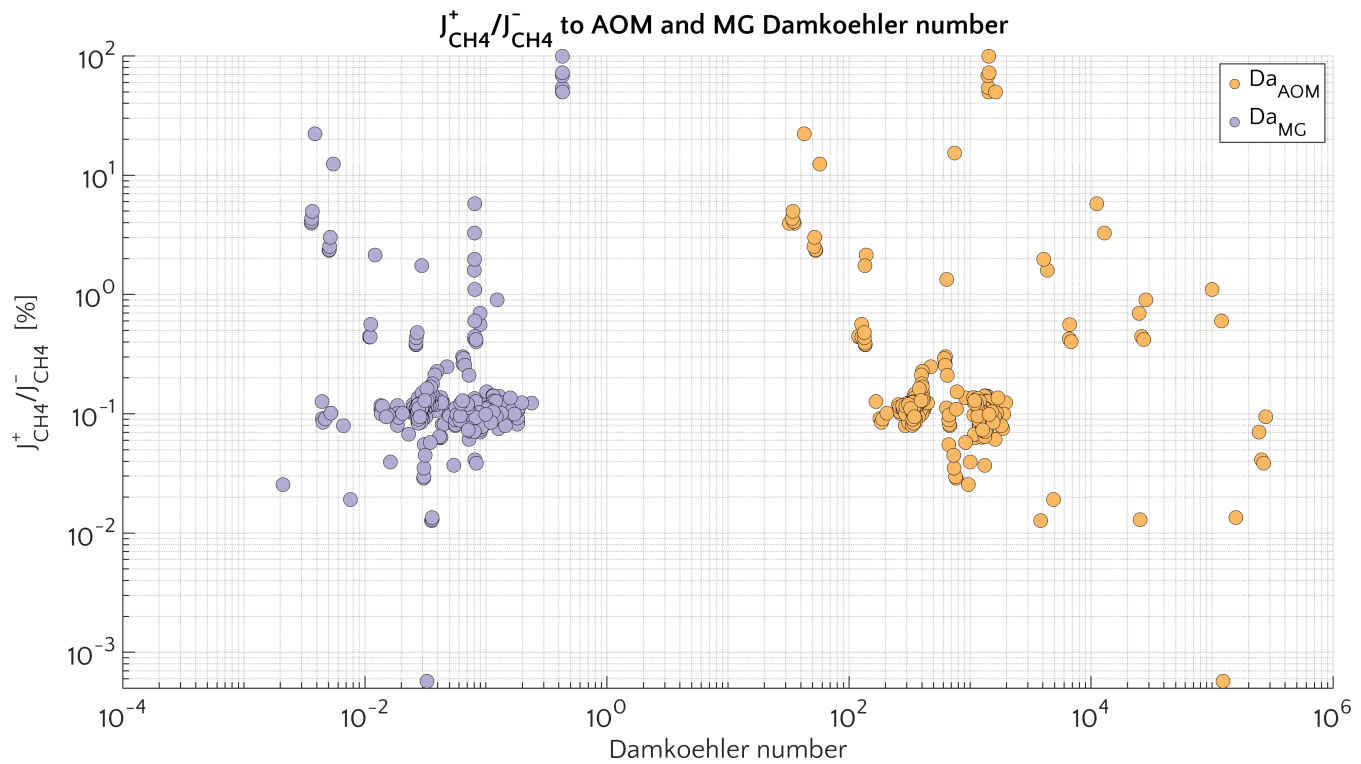


Figure S2. Ratio $J_{CH_4}^+ / J_{CH_4}^-$ (in %) as a function pf the Damköler numbers for AOM (orange) and for methanogenesis (purple)

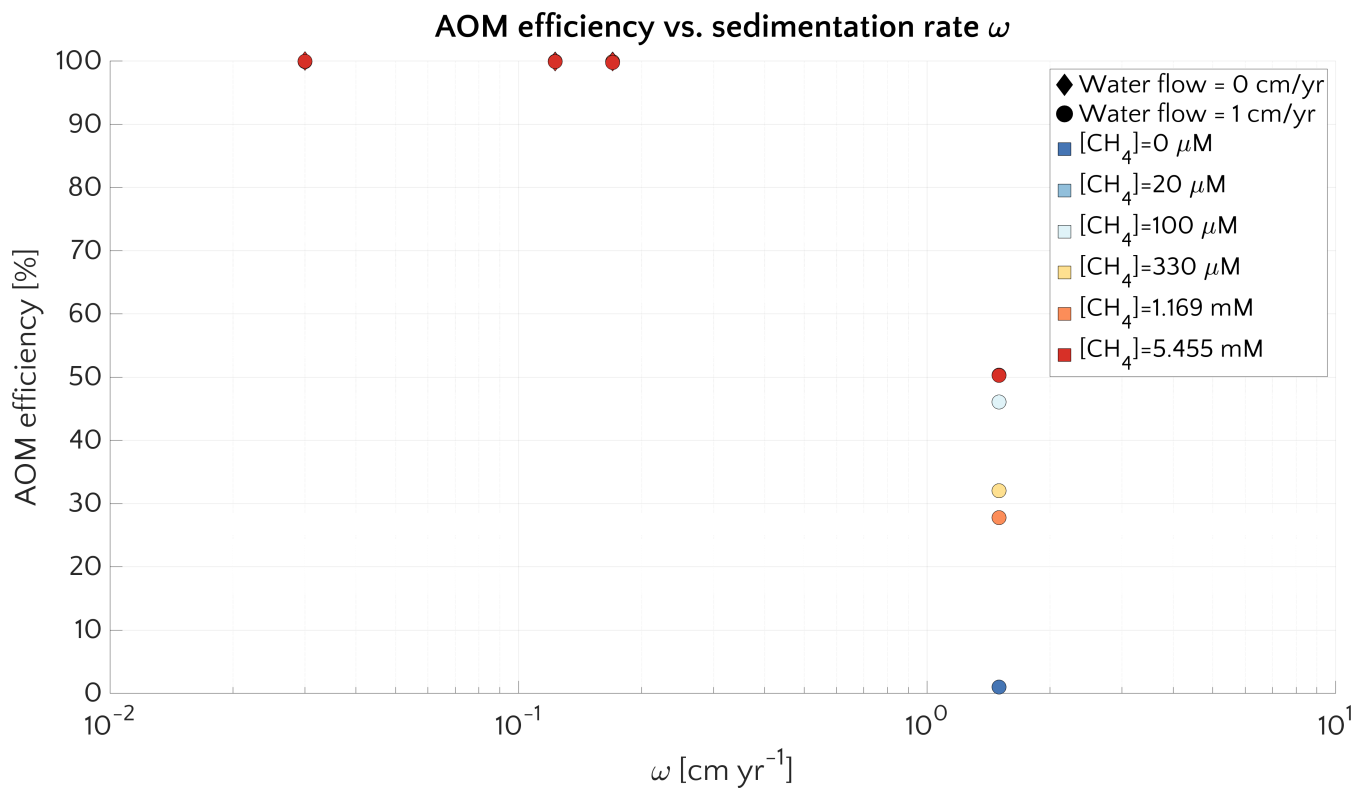


Figure S3. AOM filter efficiency η versus ω for passive cases (diamonds) and active cases (circles).

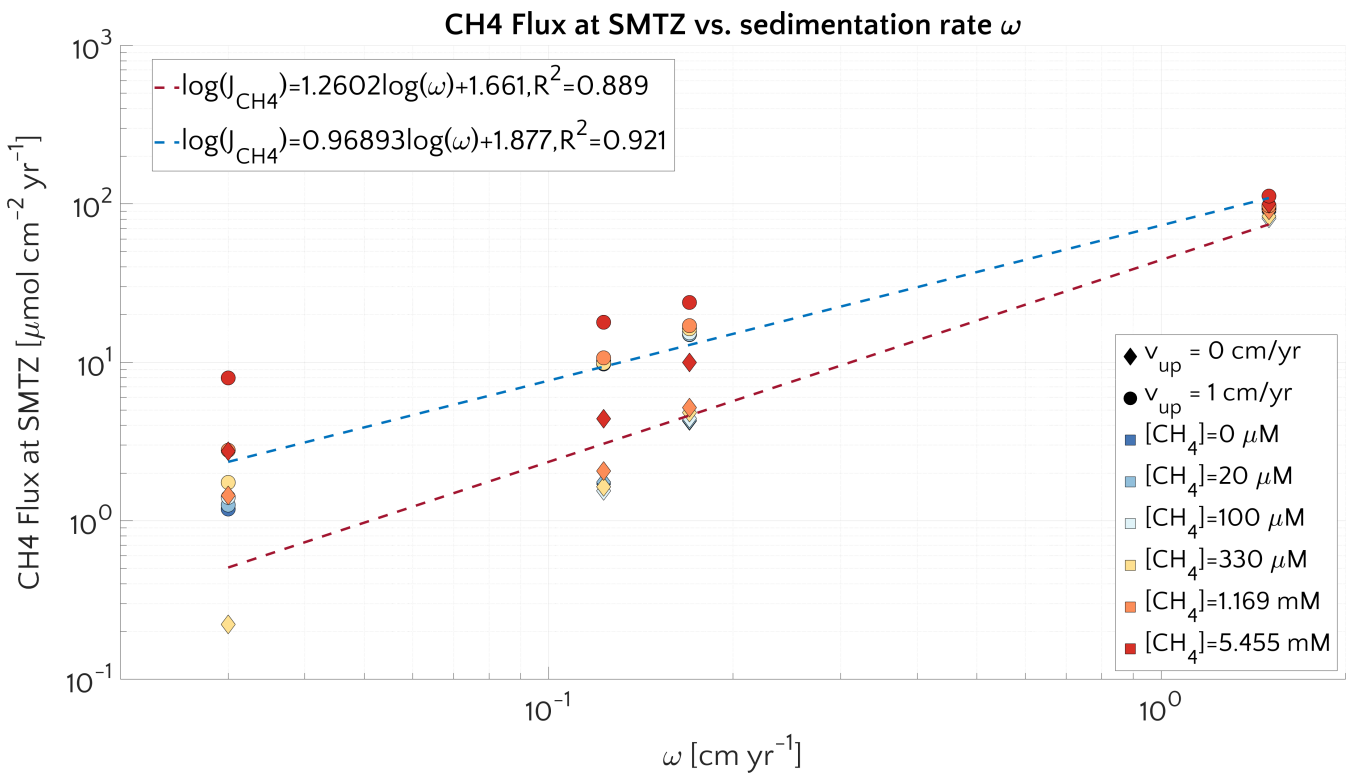


Figure S4. Methane flux at the centre of SMTZ versus ω for passive (diamonds) and active (circle) cases. Log-log fit is reported.

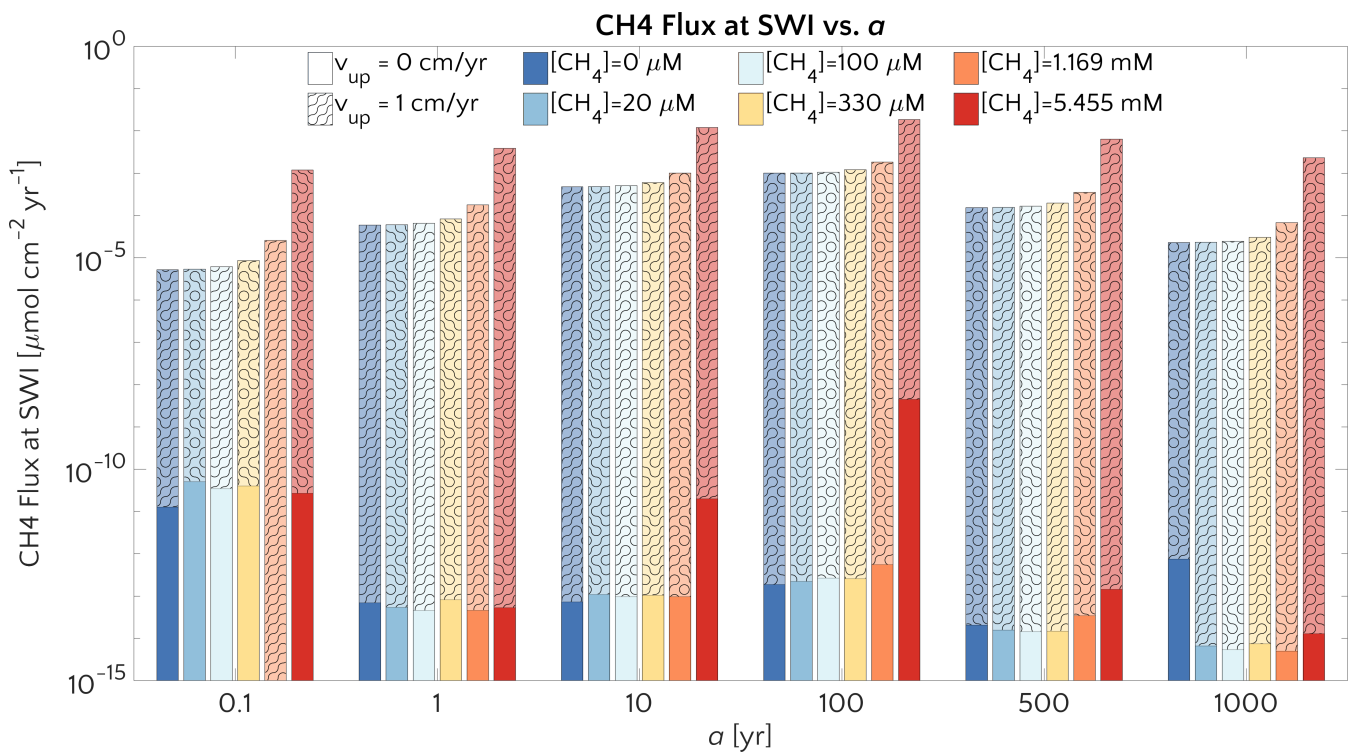


Figure S5. Barplot of the methane flux at the SWI versus α for passive case (plain) and active case (pattern) and the $[\text{CH}_4]_-$ reported in the text.

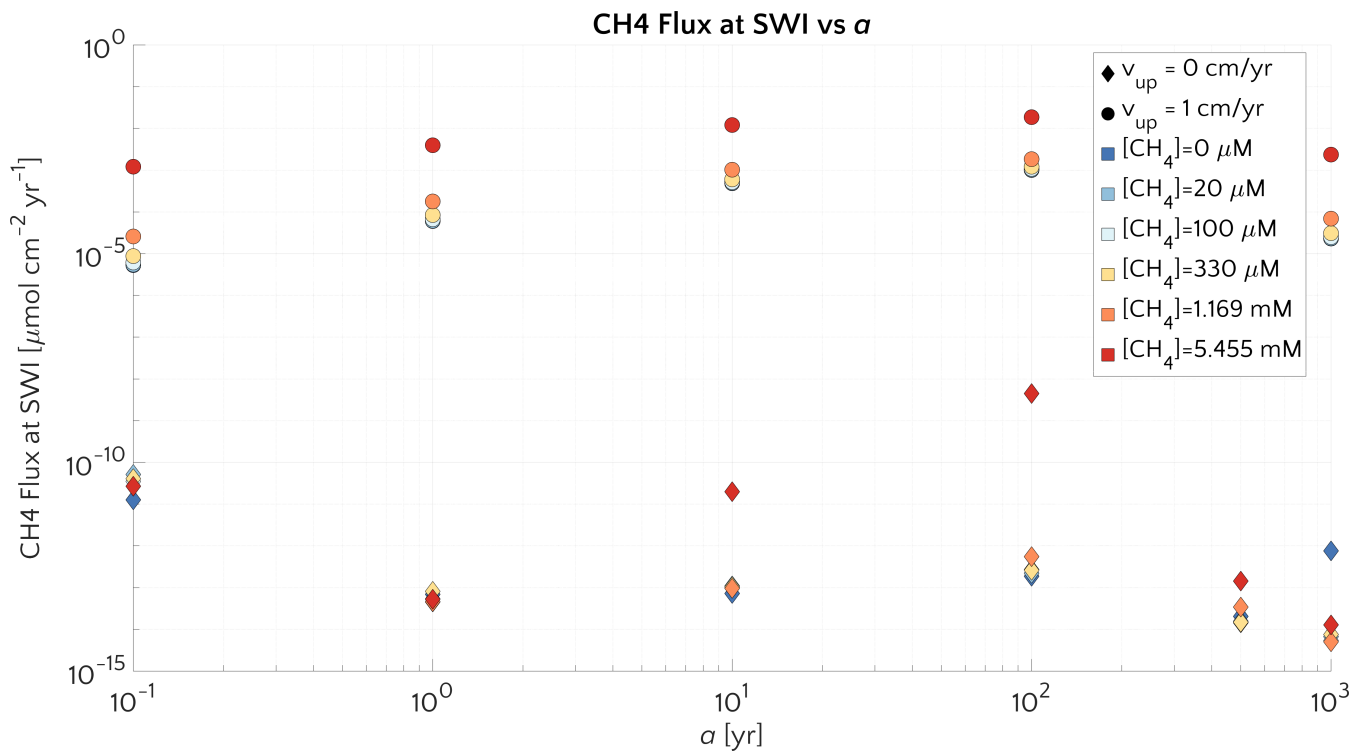


Figure S6. Methane flux at SWI versus α for passive (diamonds) and active (circle) cases.

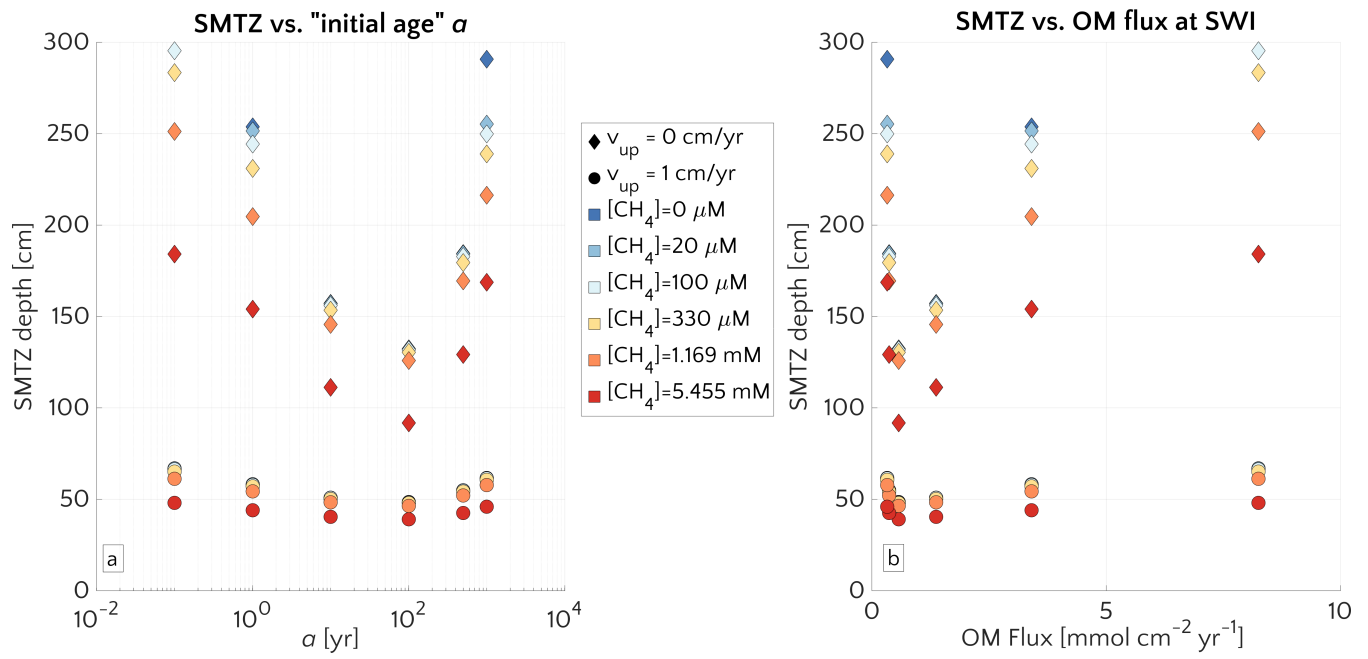
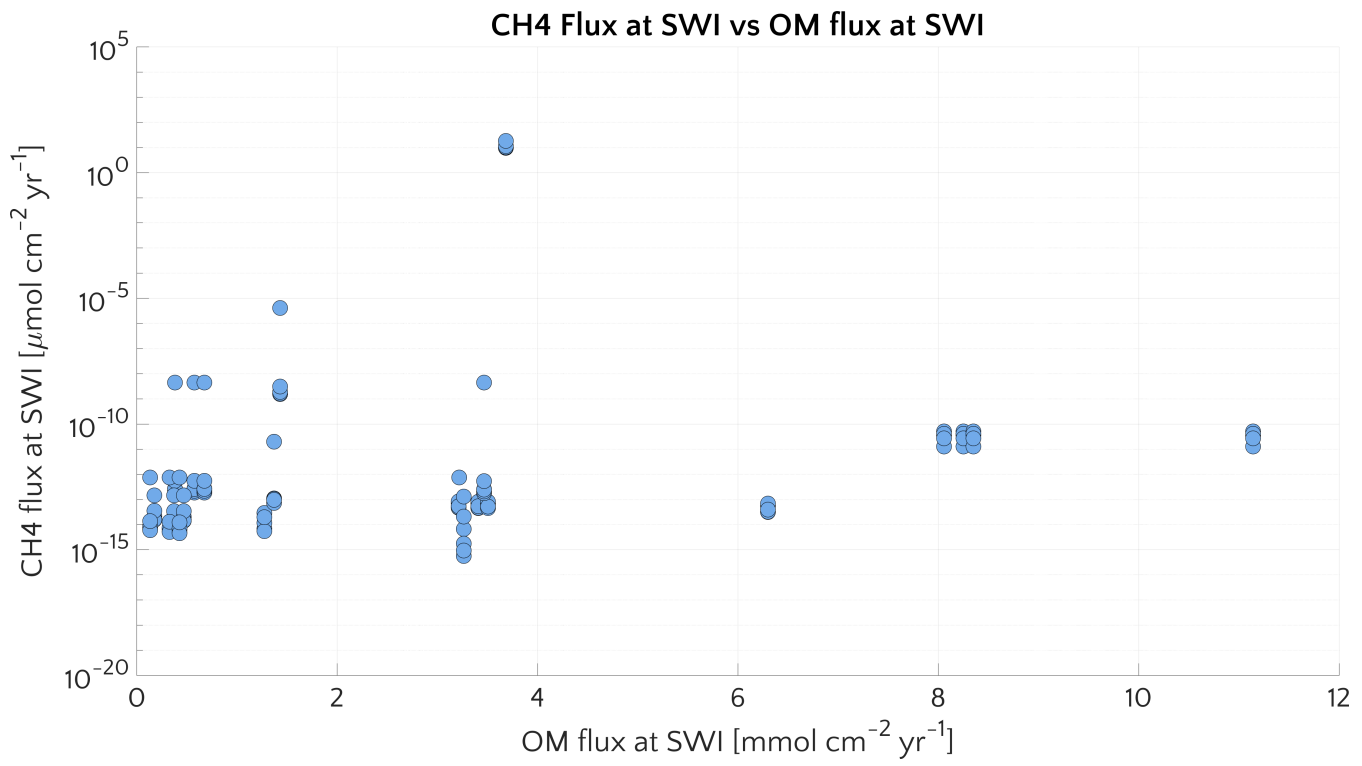


Figure S7. (a) SMTZ depth versus α . Passive (diamonds) and active (circle) cases for different $[CH_4]_-$. (b) SMTZ depth versus OM flux entering the system at the SWI.



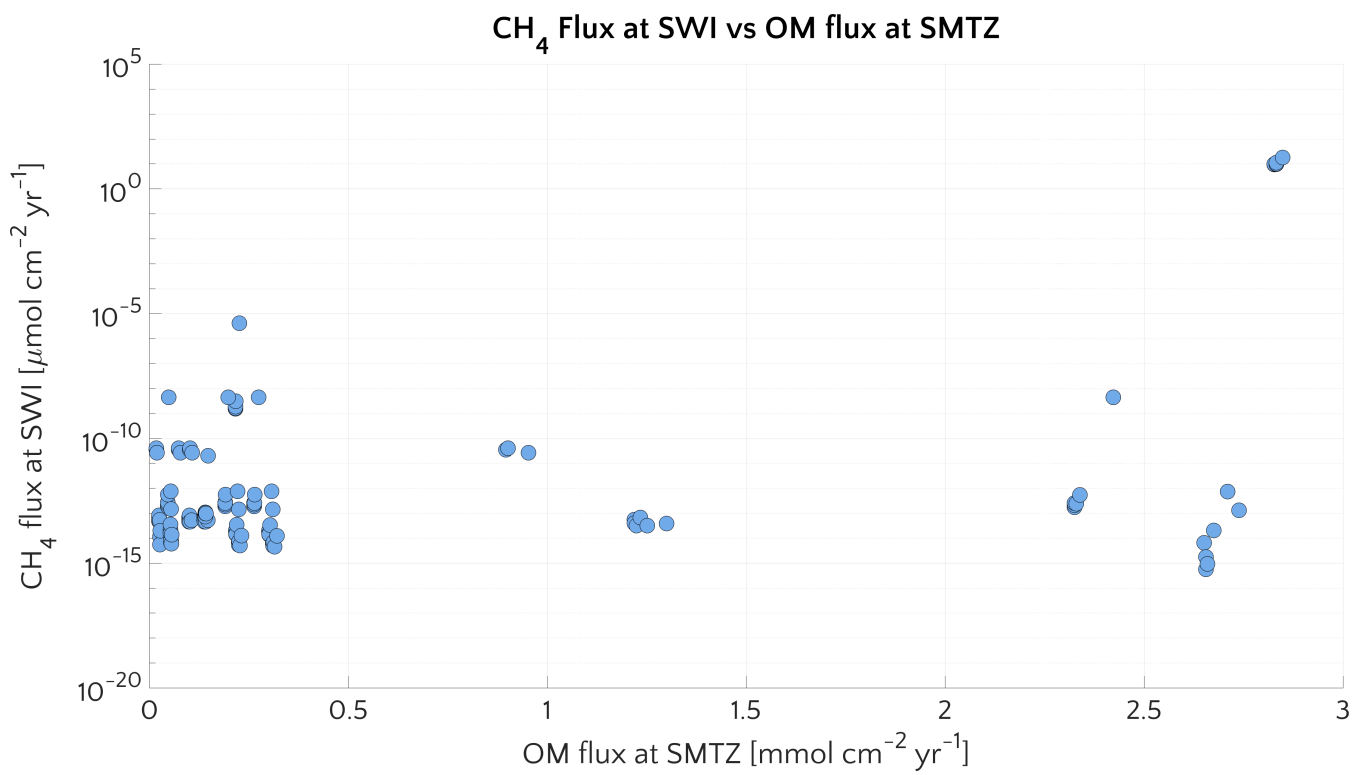


Figure S9. Methane flux at SWI versus OM flux at SMTZ

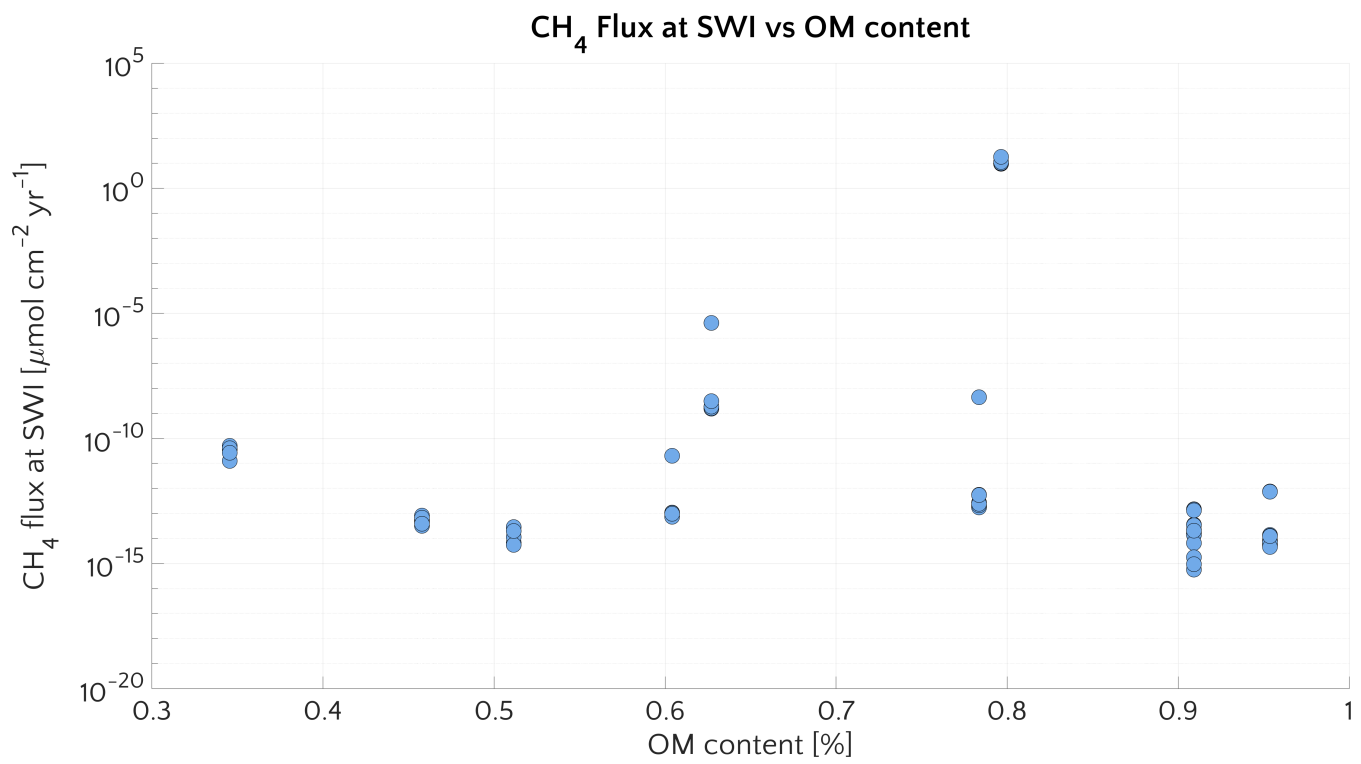


Figure S10. Methane flux at SWI versus OM sediment content

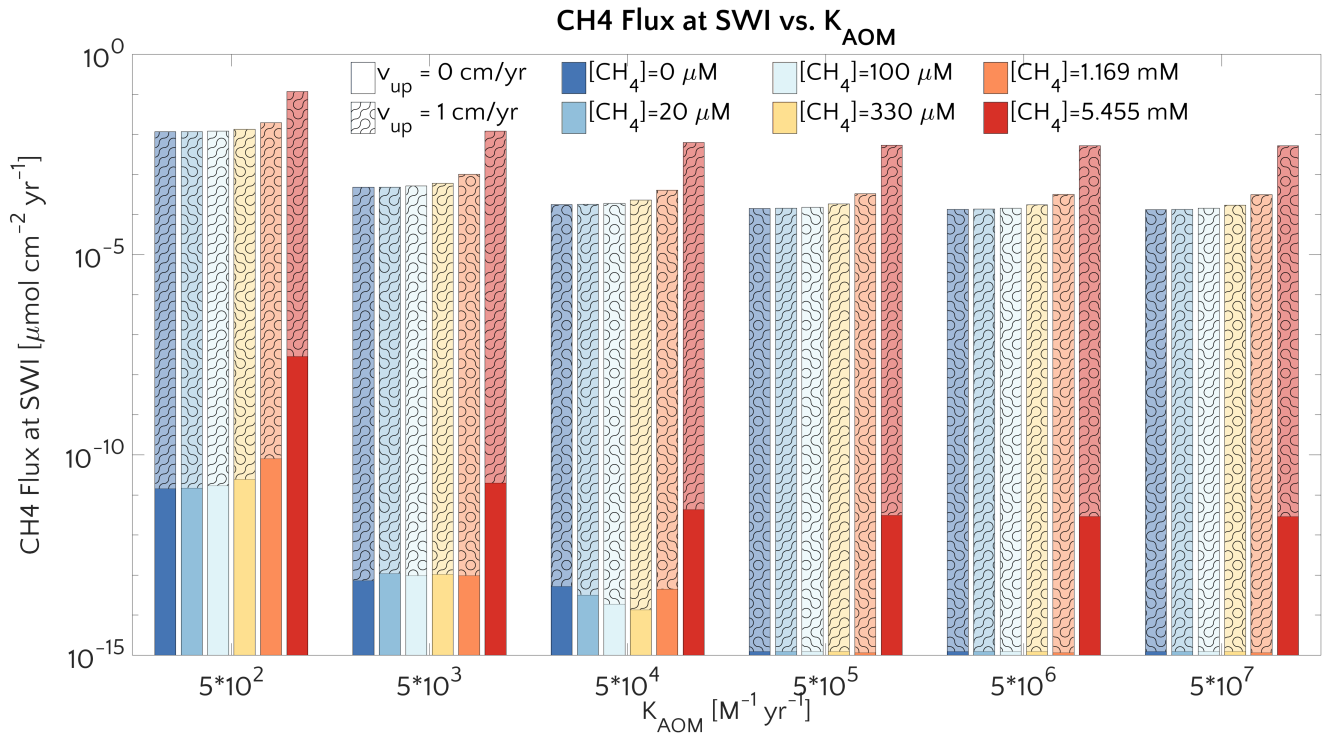


Figure S11. Methane flux at SWI versus AOM reactivity constant k_{AOM}

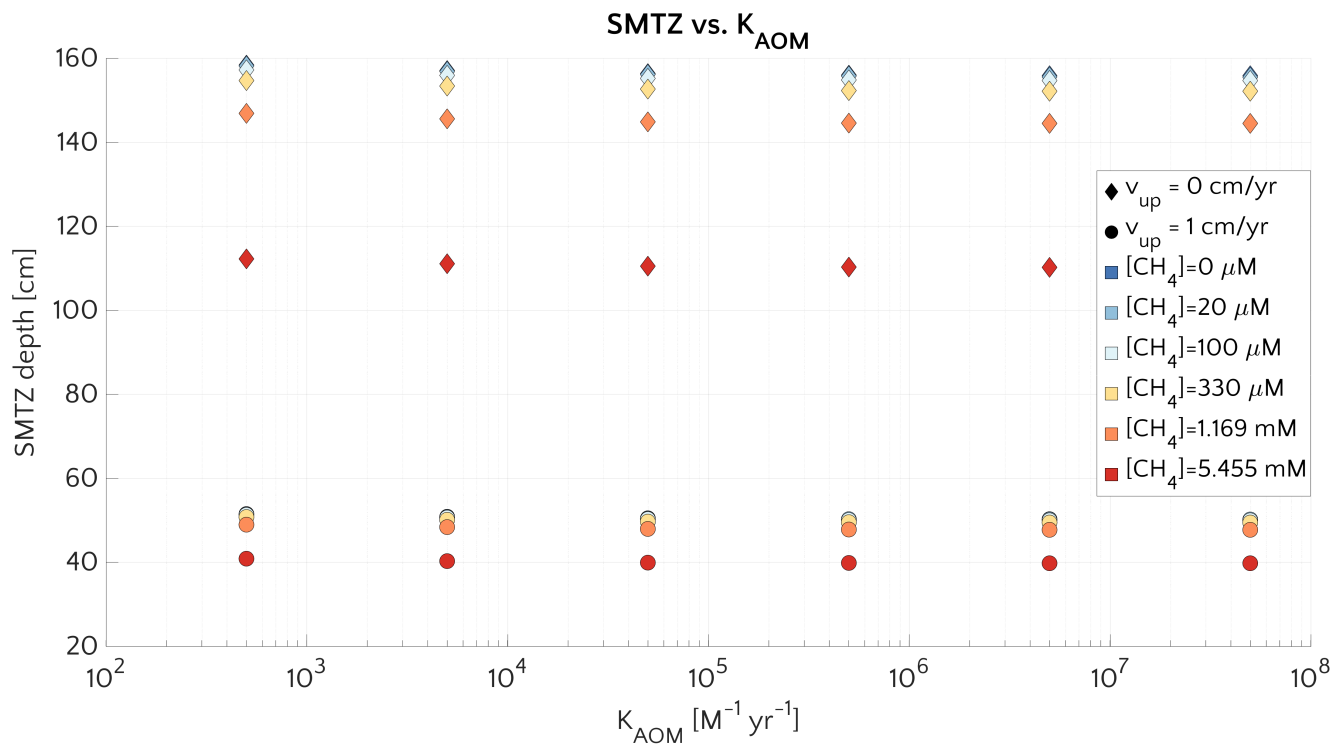


Figure S12. SMTZ depth versus k_{AOM} . Passive (diamonds) and active (circle) cases for different $[CH_4]_-$.

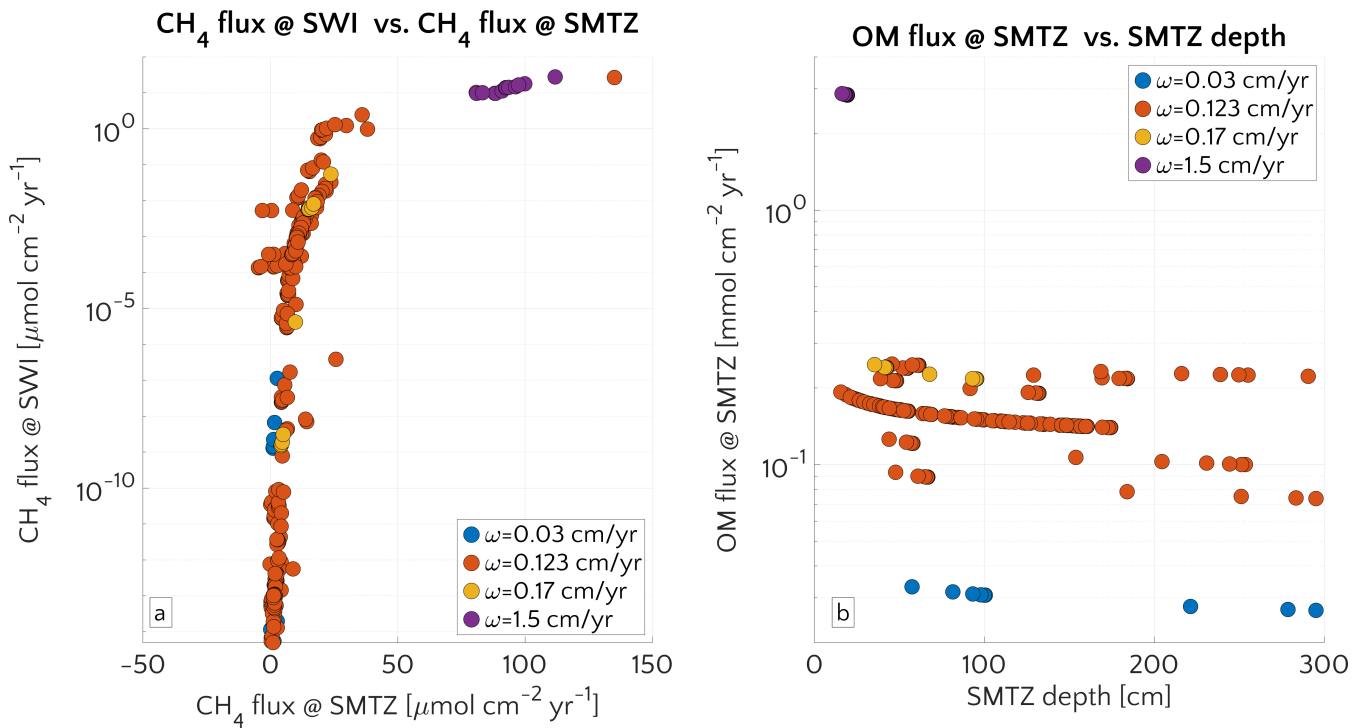


Figure S13. *a.* Flux of methane at SWI versus flux of methane at the SMTZ depth. *b.* OM flux at the SMTZ depth versus SMTZ depth itself. Colours identify simulations with different ω .

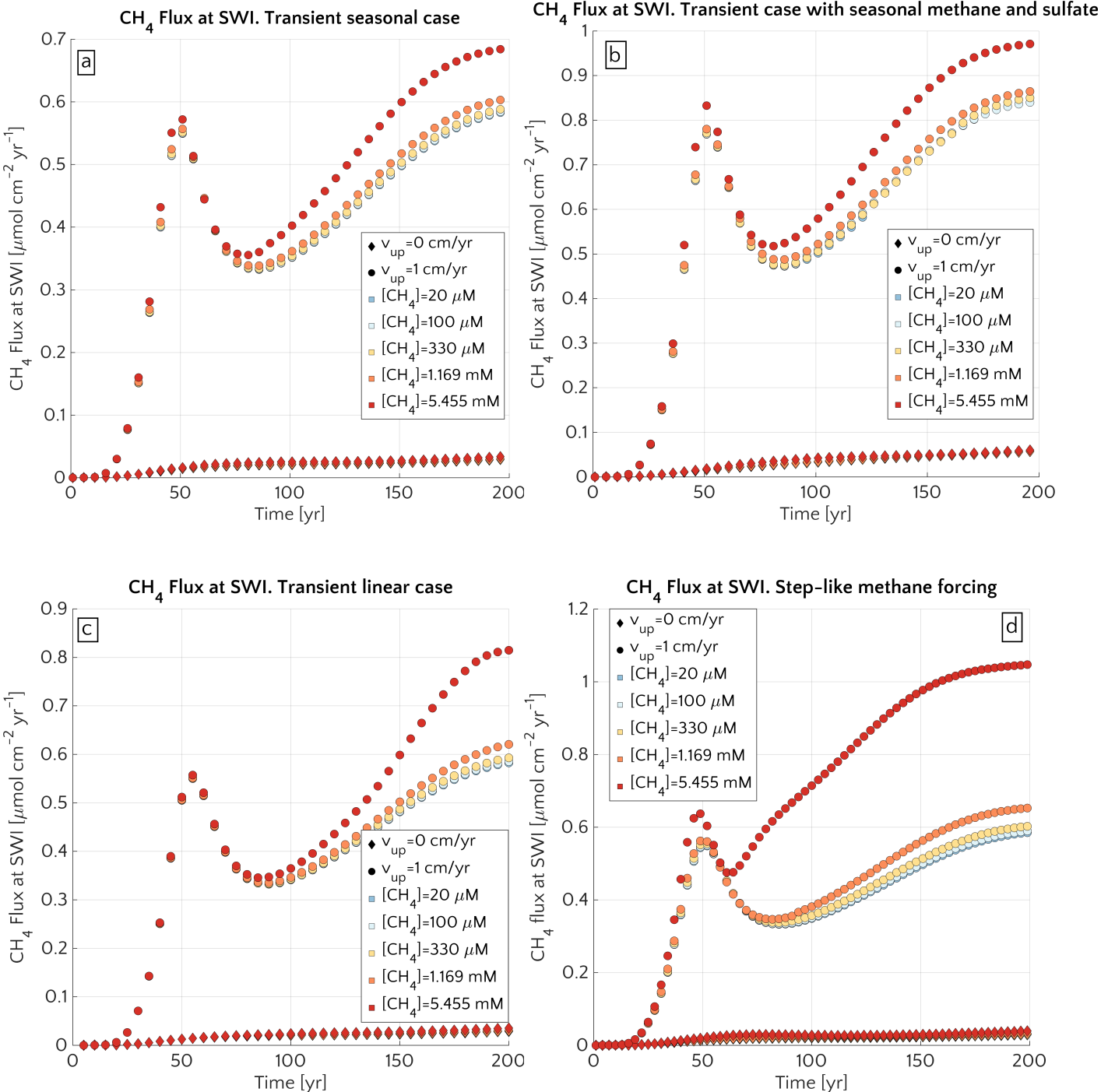


Figure S14. Flux of methane at SWI over time for passive (diamonds) and active (circle) setups and different $[CH_4]_-$. *a.* Seasonal methane forcing from below. *b.* Seasonal methane forcing from below and seasonal sulfate forcing from above. *c.* Linear methane forcing from below. *d.* Step-like methane forcing from below.

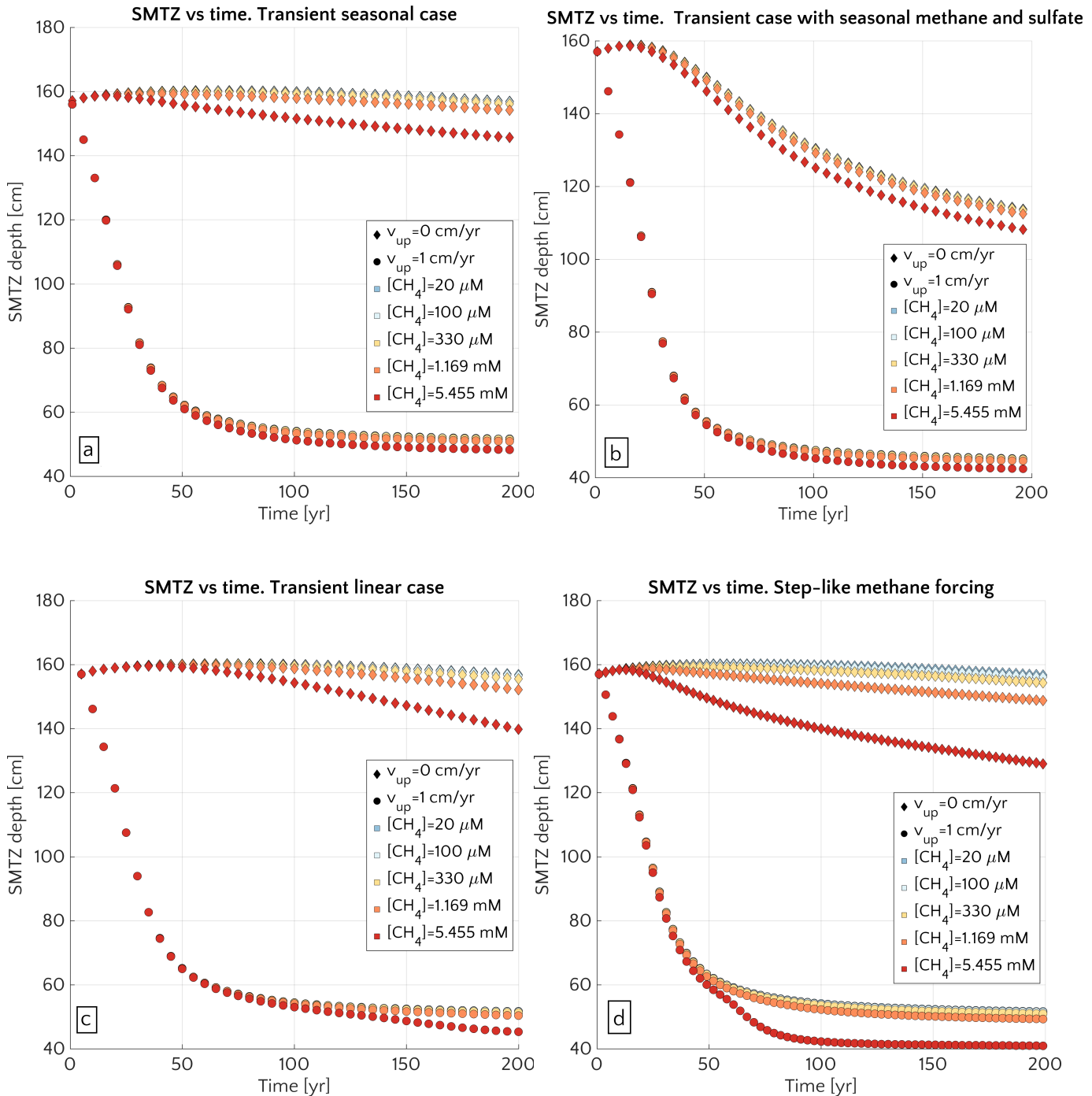


Figure S15. Movement of SMTZ over time for passive (diamonds) and active (circle) setups and different $[CH_4]_-$. *a.* Seasonal methane forcing from below. *b.* Seasonal methane forcing from below and seasonal sulfate forcing from above. *c.* Linear methane forcing from below. *c.* Step-like methane forcing from below.

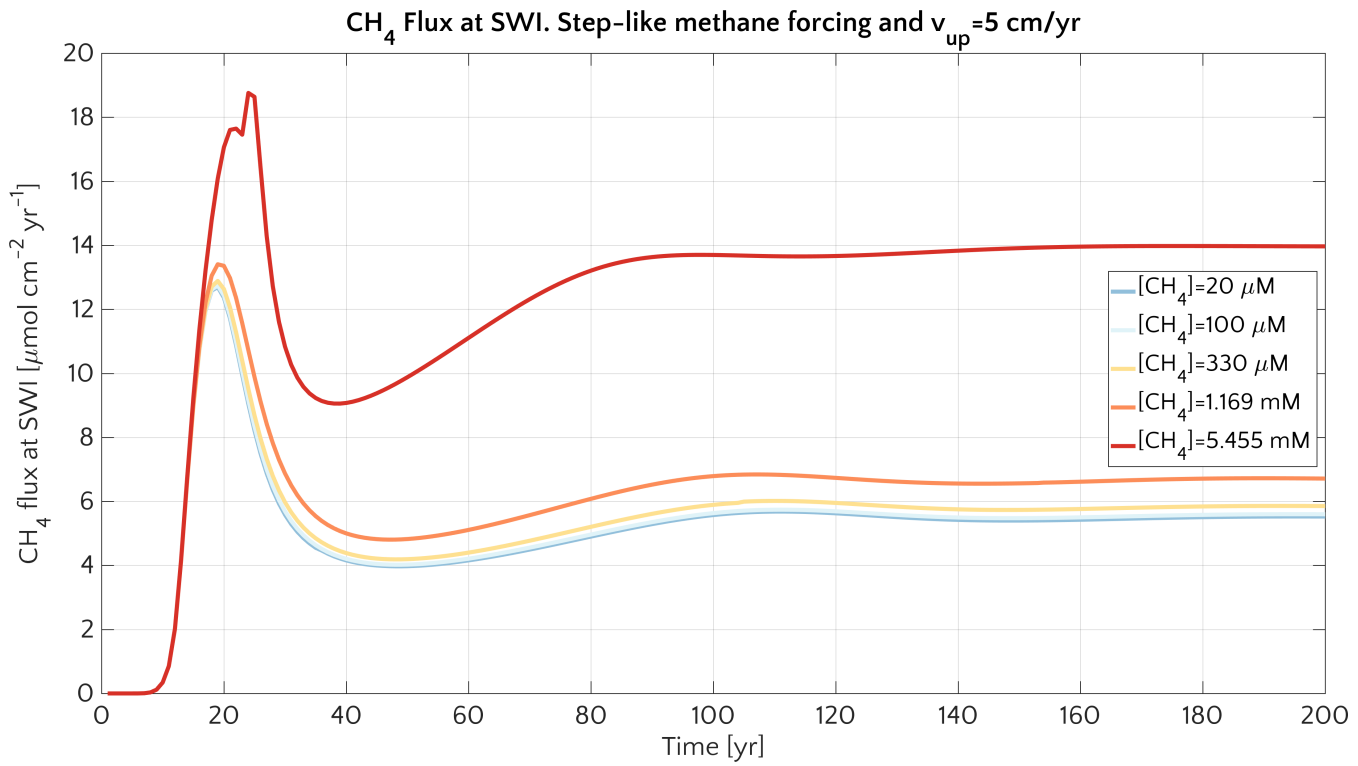


Figure S16. Flux of methane at SWI versus time for scenario 4 (step-like methane increase) and $v_{up} = 5 \text{ cm/yr}$. Colours identify simulations with different CH_4 bottom concentrations.

Integrated AOM vs bottom CH_4 concentration

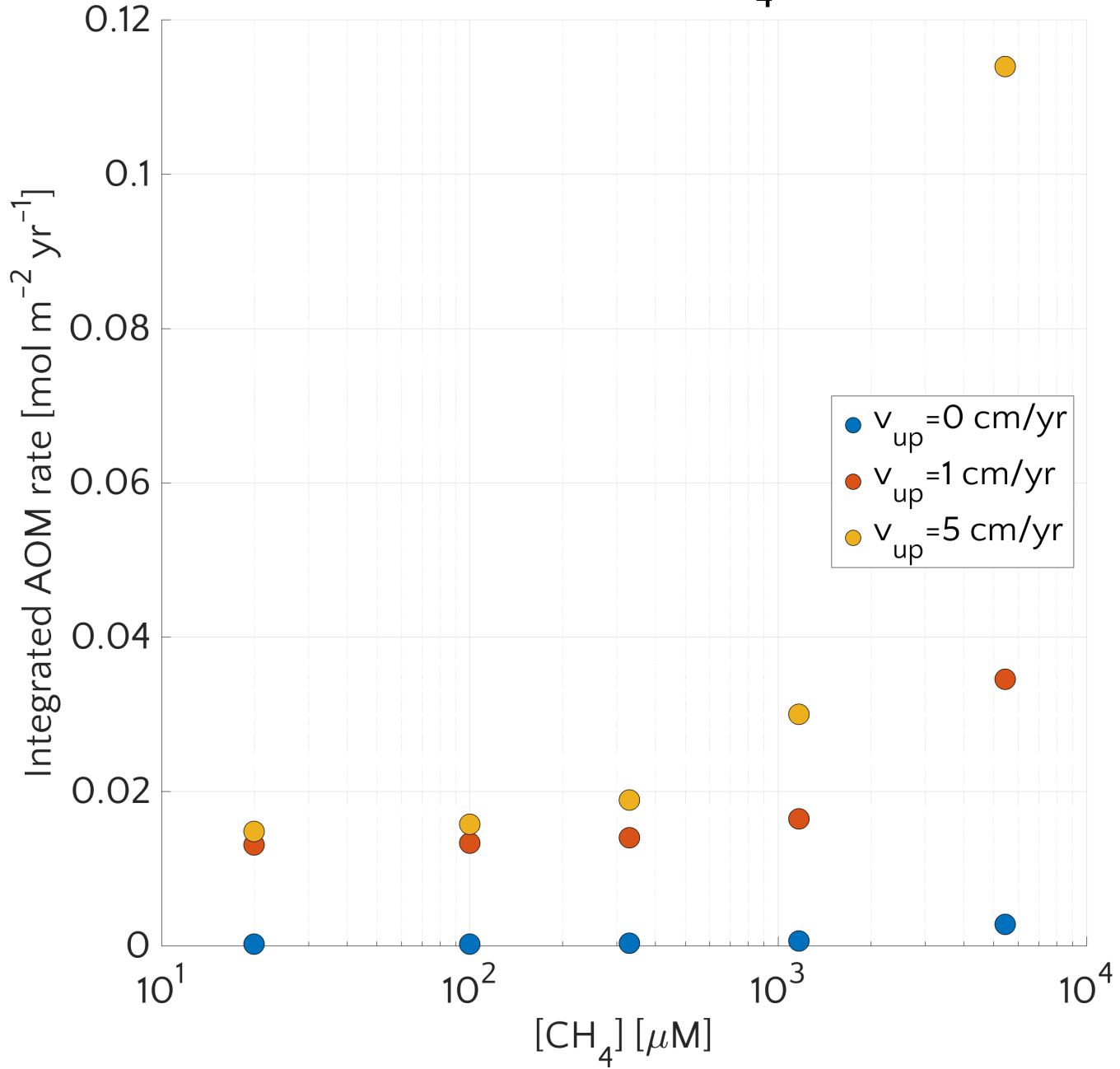


Figure S17. Vertically integrated AOM vs the bottom methane concentration $[\text{CH}_4]_-$ for three different v_{up} .

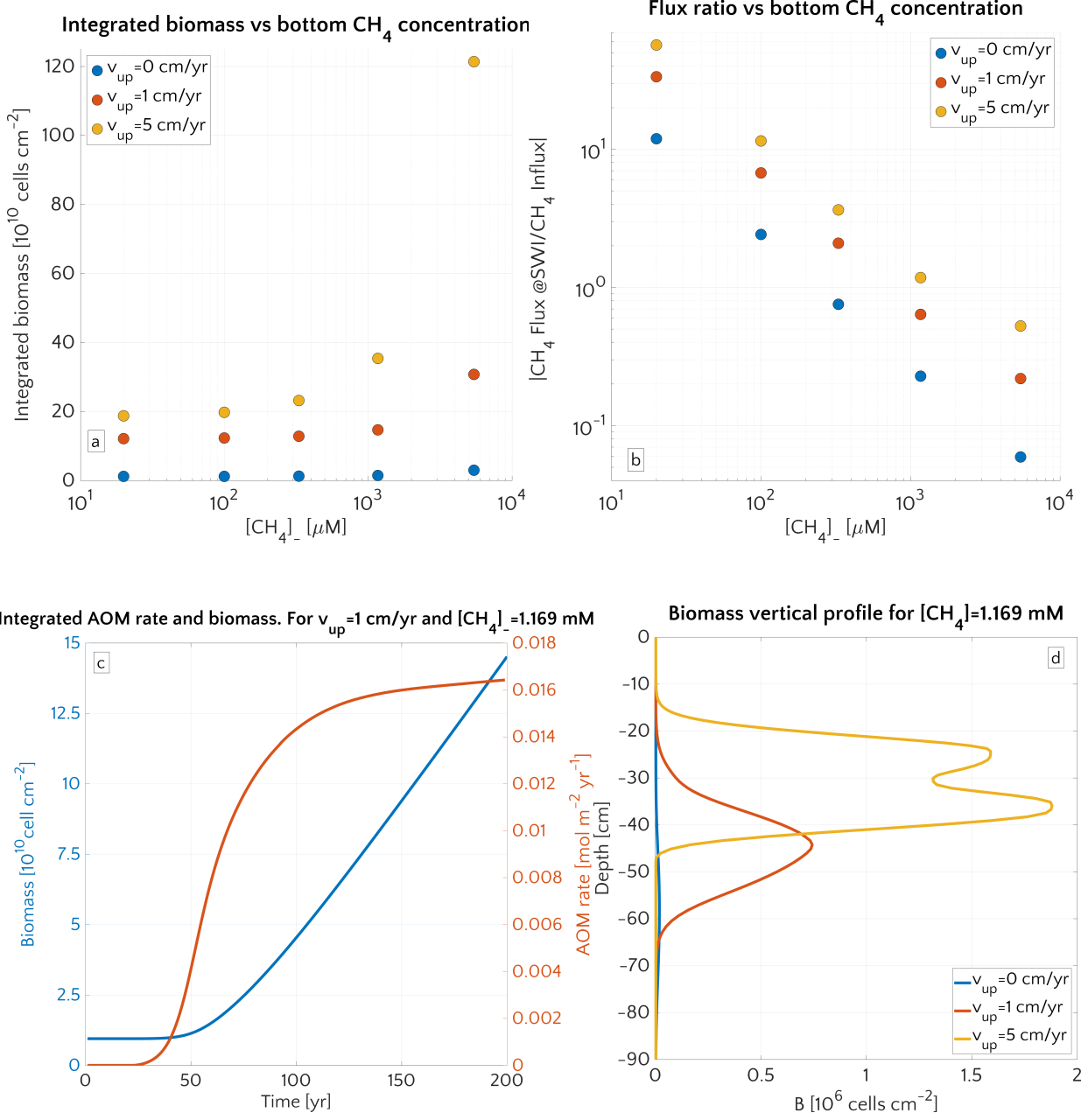


Figure S18. *a.* Vertically integrated biomass after 200 years vs the bottom methane concentration $[\text{CH}_4]_-$ for three different v_{up} . *b.* Absolute value of the ratio of the methane flux at the SWI to the advective methane flux at the base of sediment column vs the bottom methane concentration $[\text{CH}_4]_-$ for three different v_{up} . *c.* Time evolution of the vertically integrated AOM biomass (blue) and vertically integrated AOM rate (red) for the step-like simulation with $[\text{CH}_4]_- = 1.169 \text{ mM}$ and $v_{\text{up}} = 1 \text{ cm/yr}$. *d.* AOM biomass vertical profile after 200 years for three different v_{up} in case of step-like simulation with $[\text{CH}_4]_- = 1.169 \text{ mM}$.

References

- Aller, R. C. and Blair, N. E.: Early diagenetic remineralization of sedimentary organic C in the Gulf of Papua deltaic complex (Papua New Guinea): net loss of terrestrial C and diagenetic fractionation of C isotopes, *Geochimica et Cosmochimica Acta*, 68, 1815–1825, 2004.
- Arndt, S., Jørgensen, B. B., LaRowe, D. E., Middelburg, J., Pancost, R., and Regnier, P.: Quantifying the degradation of organic matter in marine sediments: a review and synthesis, *Earth-science reviews*, 123, 53–86, 2013.
- Athy, L. F.: Density, porosity, and compaction of sedimentary rocks, *AAPG Bulletin*, 14, 1–24, 1930.
- Bauch, H. A., Mueller-Lupp, T., Taldenkova, E., Spielhagen, R. F., Kassens, H., Grootes, P. M., Thiede, J., Heinemeier, J., and Petryashov, V.: Chronology of the Holocene transgression at the North Siberian margin, *Global and Planetary Change*, 31, 125–139, 2001.
- Berg, P.: Dynamic Modeling of Early Diagenesis and Nutrient Cycling. A Case Study in an Artic Marine Sediment, *American Journal of Science*, 303, 905–955, 2003.
- Berner, R. A.: Early diagenesis: a theoretical approach, 1, Princeton University Press, 1980.
- Boudreau, B. P.: Diagenetic models and their implementation, vol. 505, Springer Berlin, 1997.
- Boudreau, B. P. and Ruddick, B. R.: On a reactive continuum representation of organic matter diagenesis, *American Journal of Science*, 291, 507–538, 1991.
- Claypool, G. E. and Kaplan, I.: The origin and distribution of methane in marine sediments, in: *Natural gases in marine sediments*, pp. 99–139, Springer, 1974.
- Dale, A. W., Regnier, P., and Van Cappellen, P.: Bioenergetic controls on anaerobic oxidation of methane (AOM) in coastal marine sediments: a theoretical analysis, *American Journal of Science*, 306, 246–294, 2006.
- Dale, A. W., Aguilera, D., Regnier, P., Fossing, H., Knab, N., and Jørgensen, B. B.: Seasonal dynamics of the depth and rate of anaerobic oxidation of methane in Aarhus Bay (Denmark) sediments, *Journal of Marine Research*, 66, 127–155, 2008a.
- Dale, A. W., Van Cappellen, P., Aguilera, D., and Regnier, P.: Methane efflux from marine sediments in passive and active margins: Estimations from bioenergetic reaction–transport simulations, *Earth and Planetary Science Letters*, 265, 329–344, 2008b.
- Dale, A. W., Meyers, S. R., Aguilera, D. R., Arndt, S., and Wallmann, K.: Controls on organic carbon and molybdenum accumulation in Cretaceous marine sediments from the Cenomanian–Turonian interval including Oceanic Anoxic Event 2, *Chemical Geology*, 324–325, 28–45, 2012.
- Dale, A. W., Nickelsen, L., Scholz, F., Hensen, C., Oschlies, A., and Wallmann, K.: A revised global estimate of dissolved iron fluxes from marine sediments, *Global Biogeochemical Cycles*, 29, 691–707, <https://doi.org/10.1002/2014gb005017>, <https://doi.org/10.1002/2F2014gb005017>, 2015.
- Froelich, P., Klinkhammer, G., Bender, M. L., Luedtke, N., Heath, G. R., Cullen, D., Dauphin, P., Hammond, D., Hartman, B., and Maynard, V.: Early oxidation of organic matter in pelagic sediments of the eastern equatorial Atlantic: suboxic diagenesis, *Geochimica et cosmochimica acta*, 43, 1075–1090, 1979.
- Garcia, H. E., Boyer, T. P., Locarnini, R. A., Antonov, J. I., Mishonov, A. V., Baranova, O. K., Zweng, M. M., Reagan, J. R., Johnson, D. R., and Levitus, S.: World Ocean Atlas 2009, Volume 3: Dissolved Oxygen, Apparent Oxygen Utilization, and Oxygen Saturation, 2010a.
- Garcia, H. E., Locarnini, R. A., Boyer, T. P., Antonov, J. I., Baranova, O. K., Zweng, M. M., Reagan, J. R., Johnson, D. R., Mishonov, A. V., and Levitus, S.: World Ocean Atlas 2009, Volume 4: Nutrients (phosphate, nitrate, silicate), 2010b.
- Glasby, G. P.: Manganese: predominant role of nodules and crusts, in: *Marine geochemistry*, pp. 371–427, Springer, 2006.
- Han, P.: Characteristics and sedimentation rates at the shallow Laptev Sea, Master's thesis, University of Bremen, 2014.

- LaRowe, D. E., Burwicz, E., Arndt, S., Dale, A. W., and Amend, J. P.: Temperature and volume of global marine sediments, *Geology*, 45, 275–278, 2017.
- Meile, C. and Van Cappellen, P.: Particle age distributions and O₂ exposure times: Timescales in bioturbated sediments, *Global biogeochemical cycles*, 19, 2005.
- 5 Middelburg, J. J., Soetaert, K., and Herman, P. M.: Empirical relationships for use in global diagenetic models, *Deep Sea Research Part I: Oceanographic Research Papers*, 44, 327–344, 1997.
- Millero, F. J.: Thermodynamics of the carbon dioxide system in the oceans, *Geochimica et Cosmochimica Acta*, 59, 661–677, [https://doi.org/10.1016/0016-7037\(94\)00354-o](https://doi.org/10.1016/0016-7037(94)00354-o), <https://doi.org/10.1016%2F0016-7037%2894%2900354-o>, 1995.
- Mucci, A.: The solubility of calcite and aragonite in seawater at various salinities, temperatures, and one atmosphere total pressure, *American Journal of Science*, 283, 780–799, <https://doi.org/10.2475/ajs.283.7.780>, <https://doi.org/10.2475%2Fajs.283.7.780>, 1983.
- 10 Pauss, A., Andre, G., Perrier, M., and Guiot, S. R.: Liquid-to-gas mass transfer in anaerobic processes: inevitable transfer limitations of methane and hydrogen in the biomethanation process, *Appl. Environ. Microbiol.*, 56, 1636–1644, 1990.
- Regnier, P., Dale, A. W., Arndt, S., LaRowe, D., Mogollón, J., and Van Cappellen, P.: Quantitative analysis of anaerobic oxidation of methane (AOM) in marine sediments: a modeling perspective, *Earth-Science Reviews*, 106, 105–130, 2011.
- 15 Sales de Freitas, F.: Deciphering the relationships between reactivity and sources of organic matter in marine sediments: a coupled large-scale model and lipid biomarker analysis, Ph.D. thesis, School on Earth Sciences, University of Bristol, 2018.
- Sauer, S., Knies, J., Lepland, A., Chand, S., Eichinger, F., and Schubert, C. J.: Hydrocarbon sources of cold seeps off the Vesterålen coast, northern Norway, *Chemical Geology*, 417, 371–382, 2015.
- Sauer, S., Hong, W.-L., Knies, J., Lepland, A., Forwick, M., Klug, M., Eichinger, F., Baranwal, S., Crémère, A., Chand, S., et al.: Sources 20 and turnover of organic carbon and methane in fjord and shelf sediments off northern Norway, *Geochemistry, Geophysics, Geosystems*, 17, 4011–4031, 2016.
- Stein, R. and Fahl, K.: Holocene accumulation of organic carbon at the Laptev Sea continental margin (Arctic Ocean): sources, pathways, and sinks, *Geo-Marine Letters*, 20, 27–36, <https://doi.org/10.1007/s003670000028>, <https://doi.org/10.1007%2Fs003670000028>, 2000.
- Stein, R., Boucsein, B., Fahl, K., de Oteyza, T. G., Knies, J., and Niessen, F.: Accumulation of particulate organic carbon at the Eurasian 25 continental margin during late Quaternary times: controlling mechanisms and paleoenvironmental significance, *Global and Planetary Change*, 31, 87–104, 2001.
- Stumm, W. and Morgan, J. J.: *Aquatic Chemistry: Chemical Equilibria and Rates in Natural Waters {Environmental Science and Technology}*, Wiley, 1996.
- Thullner, M., Dale, A. W., and Regnier, P.: Global-scale quantification of mineralization pathways in marine sediments: A reaction-transport 30 modeling approach, *Geochemistry, geophysics, geosystems*, 10, 2009.
- Van Cappellen, P. and Wang, Y.: Cycling of iron and manganese in surface sediments; a general theory for the coupled transport and reaction of carbon, oxygen, nitrogen, sulfur, iron, and manganese, *American Journal of Science*, 296, 197–243, 1996.
- Wallmann, K., Aloisi, G., Haeckel, M., Obzhirov, A., Pavlova, G., and Tishchenko, P.: Kinetics of organic matter degradation, microbial methane generation, and gas hydrate formation in anoxic marine sediments, *Geochimica et Cosmochimica Acta*, 70, 3905–3927, 2006.